1976

Infrared Photoconductivity in Thin Silver Sulfide Films

Paul Joseph Aceto
University of Rhode Island

INFRARED PHOTOCONDUCTIVITY IN THIN SILVER SULFIDE FILMS

BY

PAUL JOSEPH ACETO

A THESIS SUBMITTED IN PARTIAL FULFILLMENT OF THE REQUIREMENTS FOR THE DEGREE OF

MASTER OF SCIENCE

IN

ELECTRICAL ENGINEERING

UNIVERSITY OF RHODE ISLAND

1976

MASTER OF SCIENCE THESIS

OF

PAUL JOSEPH ACETO

Approved:

Thesis Committee

Major Professor S. Mardin

Anton F. Hohenheim

William J. Penhallow

G. Sadasiv

J. A. Michel

Dean of the Graduate School

UNIVERSITY OF RHODE ISLAND

1976

ABSTRACT

A study of thermally generated conductivity and photoconductivity in thin layers of silver sulfide is presented.

Silver layers were vacuum deposited on sapphire substrates and transformed into silver sulfide in a sulfur atmosphere at 120° C. The dark current of single element sensors was investigated as a function of temperature and photocurrent was measured as a function of photon flux and wavelength. The samples were photosensitive to radiation in the spectral range 0.7 μm to 1.8 μm. A maximum photoresponse occured at a wavelength of 0.8 μm. The photocurrent in general increased with decreasing temperature. The absorption edge for Ag_2S at 90 K was found to be at 1.2 μm making the calculated energy gap 1.0 eV. From dark current measurements, recombination centers were found at 0.66 eV below the conduction band.

Vidicon type targets made from silver sulfide layers were also investigated and showed an image fade-out effect with a time constant in the order of seconds. Target resolution was found to exceed 10 lp/mm and the targets responded to incident photon flux levels of 30 $\mu W/cm^2$.

TABLE OF CONTENTS

LIST OF FIGURES

LIST OF SYMBOLS

c - Speed of light in a vacuum, 3×10^{8} m-s^{-1}

E - Energy, eV

E_c - Energy of bottom of conduction band, eV

E_f - Fermi level, eV

E_g - Band gap, eV

E_t - Energy difference from shallow traps to the conduction band, eV

E_r - Energy difference from recombination centers to conduction band, eV

E_v - Energy of top of valence band, eV

e - Electronic charge, 1.6×10^{-19} C

F - Photoelectron generation rate, cm^{-3}-s^{-1}

H - Photon flux density, cm^{-2}-s^{-1}

h - Planck's constant, 6.63×10^{-34} J-s

I - Current, A

I_{ph} - Photocurrent, A

j - Current density, A-cm^{-2}

k - Boltzmann's constant, 1.38×10^{-23} J-K^{-1}

N_c - Effective density of states in the conduction band, cm^{-3}

N_o - Density of recombination centers, cm^{-3}

N_t - Density of shallow traps, cm^{-3}

N_v - Effective density of states in the valence band, cm^{-3}

n - Density of electrons in the conduction band, cm^{-3}

n_r - Density of occupied recombination centers, cm^{-3}

n_t - Density of occupied shallow traps, cm^{-3}

p_r - Density of unoccupied recombination centers, cm^{-3}

s_n - Capture cross section for electrons, cm^2

T - Temperature, K

t - Time, s

v - Electronic drift velocity, $m\text{-}s^{-1}$

η - Percent of photons absorbed

λ - Wavelength, m

τ - Electronic lifetime, s

ρ - Resistivity, Ω-cm

ACKNOWLEDGMENT

I would like to thank Dr. S. Mardix for the guidance he has given me during the course of this research and for the many enlightening discussions which we have had. His keen insight and good humor have helped me through many periods of difficulty.

I would also like to thank Dr. H. Roehrig and Dr. S. Nudelman for introducing me to this field.

In addition, I wish to thank the United States Army Electronics Command, which provided part of the funds to support this project under contract number DAAB07-69-C-0420.

Finally, I which to thank Mrs. Joan Lamoureux for typing a beautiful manuscript.

INTRODUCTION

The purpose of this thesis is to describe the results of an investigation of infrared photoconductivity in thin (in the order of 1 μm) silver sulfide films. Infrared sensitive materials may be useful as both single element IR detectors and scanned, two dimensional IR detectors. Materials with a high resistivity are likely candidates for investigation of photoconductivity. This is true because high resistivity materials have a low dark current, hence low background. This low background allows for a high signal to background ratio. In addition, conductivity changes due to absorption of photons will not appreciably affect a material which already has a high conductivity. Materials with an absorption edge in the infrared are likely to be photosensitive in the IR.

Silver sulfide (Ag_2S) was known as a photoconductor as early as 1922[1]. There are two forms of Ag_2S: α-Ag_2S and β-Ag_2S. In the alpha form, Ag_2S has a body centered cubic arrangement of sulfur atoms[2] and a relatively low electrical resistivity (10^3 ohm-cm at room temperature)[3]. β-Ag_2S has a monoclinic structure[2] and a much higher resistivity (10^5 ohm-cm at room temperature)[3]. Some research has been performed on Ag_2S and it was found to have an absorption edge in the IR[4,5]. Since β-Ag_2S has a higher resistivity and

since its absorption edge is in the IR, it was chosen to be investigated in this study.

For the most part, studies of photosensitivity of Ag_2S have been carried out on chemically deposited layers[4,5,6]. The appendix details some work done at this lab on this type of layer. In the papers mentioned, the Ag_2S is formed by a reaction of organic materials and the material is allowed to precipitate onto a substrate. This method of preparation may allow spaces to form between conglomerates of crystallites of the material. These spaces may introduce undesirable effects in the photoresponse such as electric polarization within the groups of crystallites. This would lower the photocurrent. I have used an evaporation technique which produces a uniform polycrystalline layer as determined by X-ray diffraction studies done at this lab.

The thesis is divided into four main sections. The first section provides background material and develops the physical model of the band structure of Ag_2S. The second section describes the methods used to prepare the samples, the various sample geometries, the measurement techniques and the instrumentation used to study the photoconductive properties of the samples. Section three gives the experimental results of the investigation. The final section discusses the results and suggests possible future investigations and practical applications for the material.

I. THEORETICAL

An example of a semiconductor will be presented. Common intrinsic semiconductors (silicon and germanium) rely only on electrons and holes as the charge carriers. If a material has ionic bonding, ions as well as electrons may be free to move under an electric field and produce a current. Ions acted upon by a DC field will move in the direction of the field until they reach the negative electrode. Since ions cannot pass into the metal electrode, they will either build up a space charge there and polarize the sample or they will pick up an electron and neutralize. Ions acted on by an AC field will try to follow the field. If the frequency is low, the ions will oscillate. The amplitude of their oscillation will be proportional to the ionic mobility. At high enough frequencies, the amplitude of the oscillation will be small because they are too sluggish.

The electrons in a material subjected to a DC electric field will move in the opposite direction to the field. If the contacts to the sample are ohmic, electrons will pass out of the sample through the positive electrode. Electrons will be replenished via the negative electrode. An ohmic contact is one which allows electrons to flow from the material to the electrode and from the electrode to the

material equally well. In other words, an ohmic contact has a linear and symmetric current-voltage characteristic. Electrons will follow an AC field of audio and radio frequencies if they are not trapped and will not polarize the sample (as in the ionic case) due to the relatively high mobility of electrons as compared with ions.

Consider a semiconductor whose band gap ($E_g = E_c - E_v$) is in the order of one electron volt. For the moment, we will assume there are no impurity states in the gap. Electrons in the conduction band are free in the sense that they are not affected by the local fields of the nuclei and therefore can move under an external field. Electrons in the valence band cannot move under an external field. Holes in the valence band act like free electrons with a positive charge. The hole contribution to the current is assumed to be small in our case and will be neglected. At a given temperature other than 0 K, some electrons will be in the conduction band due to thermal excitation. These electrons will stay in the conduction band for a certain length of time, called the lifetime (τ), and then they will drop back down into the valence band to recombine with holes. However, there will be an equilibrium density of electrons in the conduction band because some electrons are continuously being thermally excited from the valence band while others are falling back into it. In addition to thermal excitations, the crystal may absorb a photon with sufficient energy to allow an electron to jump into the conduction band. This process also produced holes. Under constant illumination, a new

equilibrium will be established at a higher free electron density. We will assume that the hole density and mobility is small so the current is primarily due to electrons.

To this picture we now add shallow traps. These traps are energy levels in the gap close to the conduction band. An electron will be attracted to the trap and, if it falls into it, will be loosely bound to it. Since the traps are shallow, the bound electrons will be thermally re-excited into the conduction band. Electrons will not jump into the valence band from the traps because they must be freed from the traps first. The net effect of the trapping levels is to increase the electron lifetime. That is, there is a larger time between electron-hole pair creation and recombination. Electrons can spend a longer time in the conduction band by continuously being trapped and re-excited before dropping back into the valence band.

To this picture, we now add deep recombination centers. Recombination centers, as the name implies, are sites where electrons can recombine with holes. Electrons in the conduction band can jump into this centers (with an accompanying release of phonons) and remain there until they recombine with holes from the valence band. If the density of centers is large enough, electrons in them may be excited, either thermally or by photon absorption, into the conduction band. All of the above processes (thermal and photo excitation, trapping and recombination) eventually reach a dynamic equilibrium.

The following is a quantitative discussion of the material already presented. Ions in the material have a low mobility relative to electrons (due to their large mass), hence the ionic current will be smaller than the electronic current. Under an AC field at very low frequencies, the ions may traverse the entire length of the sample on each half cycle of the electric field oscillation. As the frequency is increased, the amplitude of oscillation decreases. At a high enough frequency, the ions will not move much and will not produce any appreciable current. To eliminate the ionic conduction, one need only take measurements using an AC voltage of a high enough frequency.

The following discussion of electronic conductivity assumes that the ionic conductivity can be neglected by a judicious selection of frequency. As a first approximation, assume the energy band diagram consists only of the valence band the the conduction band separated by the band gap E_g. At a temperature of absolute zero, all states in the valence band are occupied by electrons and all states in the conduction band are empty. If a voltage is applied across the material, no current will flow because there are no carriers in the conduction band. For semiconductors with no energy levels in the gap, the volume electron density (n) in the conduction band as a function of temperature is given by[7]:

$$n = N_v \exp(-E_g/2kT) \qquad (1)$$

where k is Boltzmann's constant and N_v is the effective

density of states in the valence band with the assumption that all of the states are very near the band edge. The electronic current density (j) in the material is given by[7]:

$$j = nev \tag{2}$$

where e is the electronic charge and v is the electronic drift velocity due to the electric field. For this discussion, the hole current is assumed small and is neglected. As the electronic current density and the conductivity are proportional to n, the current increases exponentially with temperature. A graph of log n vs. 1/T should give a straight line of slope $-E_g/2k$.

To this picture we now add shallow traps. These electron traps are E_t below the conduction band. If we assume recombination from these sites is negligible, the trap occupancy is given by[8]:

$$n_t = n(N_t/N_c)\exp(E_t/kT) \tag{3}$$

where n_t is the density of occupied traps, N_t is the density of traps, and N is the effective density of states in the conduction band[8]. Since we assume E_t is small as compared with kT, the traps will only act to increase the lifetime of the electrons.

Finally, we add a set of deep recombination centers at an energy E_r below the conduction band with a volume density of N_o. Since electrons from the conduction band fall into these centers, these centers may be a source of electrons (to be re-excited thermally or by absorption of

photons into the conduction band) as well as sites for recombination. If the density of recombination centers is large enough, the contribution to the free electron density from these levels may predominate over the valence band contribution. That is, if

$$\ln N_o/N_v >> \frac{|E_r - E_g|}{2kT} \tag{4}$$

the contribution to the dark current from the valence band will be negligible. In this case, the occupied recombination centers will act as the uppermost 'valence band'. In this case, the free electron density may be written as:

$$n = N_o \exp(-E_r/2kT) \tag{5}$$

If the material is illuminated, photons whose energy is less than the band gap (longer wavelength) will not excite electrons into the conduction band because they haven't got sufficient energy. If photons whose energy is greater than the band gap are absorbed by the material, electrons in the valence band will have enough energy to jump into the conduction band resulting in an increased conductivity. The wavelength at which electrons are no longer excited into the conduction band is related to the main absorption edge. An absorption edge is the wavelength at which a sharp drop in the absorption coefficient occurs. The main edge is related to the band gap. If, as in our case, there is a large density of electrons in the gap, the response will extend beyond the absorption edge. Photons which cannot produce band to band transitions due to insufficient energy may be

able to excite electrons from the recombination centers. There will be a wavelength at which these transitions will stop. This will result in a secondary absorption edge at a longer wavelength.

The following discussion of the photocurrent is a special case of the general derivation given by Rose[8]. If a sample is uniformly illuminated with light which generates photo-electrons at a constant rate (F electrons/cm^3-s) within the volume, then n, the density of photo electrons in the conduction band under steady state conditions is given by[8]:

$$n = F\tau \tag{6}$$

where τ is the lifetime of the electrons. For a material of this type, we can assume that F is approximately equal to the number of photons absorbed. We can also assume that each absorbed photon generates a free electron. Hence it can be seen that the number of photoelectrons (or the increase in conductivity) is dependent on the lifetime of electrons in the conduction band. Since the sample photocurrent is a function of n, the problem of finding an expression for current reduces to finding an expression for the lifetime.

Assume the density of unoccupied recombination centers is p_r cm^{-3}, and the capture cross section for a free electron is s_n cm^2. Consider the electron to be fixed and the recombination centers to be moving with the electron drift velocity v. In one lifetime, the centers will sweep out a volume equal to $vs_n\tau$ cm^3. The condition for capture is met

if this volume is equal to the inverse of the center's density.

$$\tau v s_n = 1/p_r \tag{7}$$

This equation is then solved for τ:

$$\tau = 1/p_r v s_n \tag{8}$$

Let us assume that the density of free plus trapped electrons ($n + n_t$) is greater than the density of unoccupied recombination centers (p_r) but smaller than the density of occupied recombination centers (n_r). Let us further assume that the density of free holes (p) is smaller than the density of free plus trapped electrons.

To recapitulate:

$$n_r > n + n_t > p_r \; ; \; n + n_t > p$$

When the sample is illuminated, p_r will change. The new value of p_r will be called the modified value, p_r'. To preserve charge neutrality, the modified unoccupied recombination center density (p_r') due to absorbed photons must be given by:

$$p_r' = n + n_t - p \tag{9}$$

Since p is small, the following approximation is valid:

$$n + n_t - p \approx n + n_t = p_r' \tag{10}$$

Now, using eq. (3) for n_t we get:

$$p_r' = n + n(N_t/N_c) \exp(E_t/kT)$$

or

$$p_r' = n(K + 1) \tag{11}$$

where $K = N_t/N_c \exp(E_t/kT)$

Now using eq. (6) and eq. (8), the density of free electrons is:

$$n = F\tau = F/p'_r\, vs_n = F/Knvs_n$$

or

$$n = \sqrt{F/Kvs_n} \tag{12}$$

Since

$$F = k_1 H \tag{13}$$

where H is the photon flux density and k_1 is a constant, and since

$$I_{ph} = k_2 n \tag{14}$$

where I_{ph} is the photocurrent and k_2 is a constant. The substitution of eq. (13) and eq. (14) into eq. (12) produces

$$I_{ph} = k\sqrt{H} \tag{15}$$

Absorption of infrared radiation, which by itself does not produce a photocurrent, can increase the photoresponse of a material. Even if the energy of a photon is too small to produce a band to band transition, it may be enough to excite electrons from the valence band directly into deep traps or recombination centers. Since the probability for an electron in the conduction band to fall into a deep state is proportional to the density of empty states (which changes), and the capture cross section (which is constant)[9], electrons are more likely to remain in the conduction band as the deep traps are filled by the infrared radiation. Since the lifetime of the electrons is increased, the photocurrent increases. This is true only if the probability for direct

recombination is smaller than the probability for recombination through recombination centers.

II. EXPERIMENTAL

The dimensions of all of the samples used are given in the following table. See Fig. 1 for sample geometries.

Sample	thickness	width	electrode separation
S1	0.55 μm	5.0 mm	7.0 mm
S2	0.55 μm	5.0 mm	7.0 mm
S4	0.55 μm	5.0 mm	1.0 mm

S6: 5.0 sq. mm, 1.0 μm between electrodes
S8: 0.2 μm thick, 2.0 mm between electrodes
T20: 0.7 μm thick, 12 mm diameter

Layer preparation:

The substrates are cleaned thoroughly before use. After boiling in acetone, they undergo several ultrasonic cleaning treatments while immersed in acetone. To remove any remaining dust particles, the substrates are dried in methanol vapors. In this method of drying, the substrate is held above a beaker of boiling methanol. When the clean vapors hit the substrate, the condense and run off, carrying dust particles with them.

After cleaning, a thin layer (5000 A to 10,000 A) of metallic silver is evaporated onto the substrate. 99.999% pure silver is used in the deposition process using an

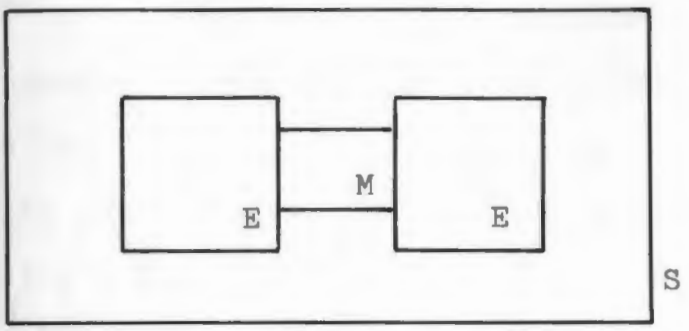

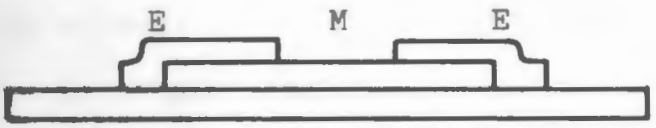

Elemental Geometry

S-sapphire substrate, E-silver electrode, M-Ag_2S, A-aluminum

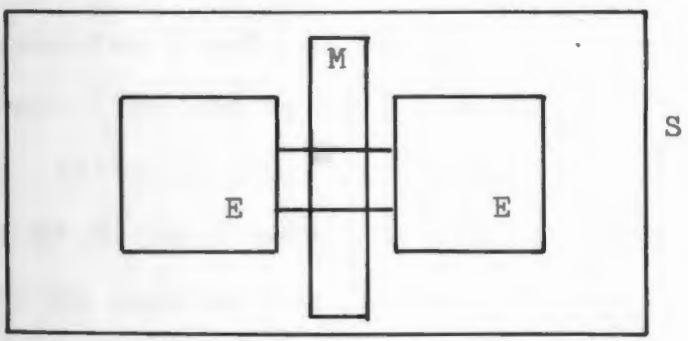

Sandwich Geometry

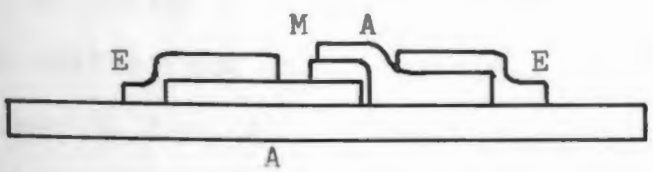

Figure 1. Sample Geometries

Edwards Speedi-Vac high vacuum coater operating at a pressure of 10^{-6} torr. These layers are transformed into silver sulfide by heating them in a sulfur atmosphere for 24 hours. Refering to Fig. 2, a metal holder (H) supports the substrate (S) in one end of a Lindburg tubular furnace (F) and a boat (B) containing 99.99% pure sulfur is placed at the other end. The furnace is heated to 120°C while an inert gas (He or Ar) passes over the boat in order to carry sulfur vapors to the silver layer. After transformation, the sample is placed in an oven at 120°C for 48 hours.

Difficulties in sample transformation:

It has been stated that the samples were kept in a sulfur atmosphere for 24 hours to transform them into Ag_2S. This interval was arrived at by trial and error. After 1 or 2 hours in the furnace, some of the material appears dull gray (Ag_2S) and some is still silvery. After 5 or 6 hours, the entire surface is dull gray. If the sample is examined with a transmitted light microscope, it appears red with black patches. The red areas are Ag_2S and the dark patches are silver. After 10 hours in the furnace, these dark patches cannot be seen under the microscope but a few sulfur crystals can be seen on the surface. At this point in time, no macroscopic amounts of silver remain in the layer. To insure thorough transformation, the samples are kept in the furnace for 24 hours.

Excess sulfur from the transformation process remains on the surface of the layers after 24 hours in the furnace.

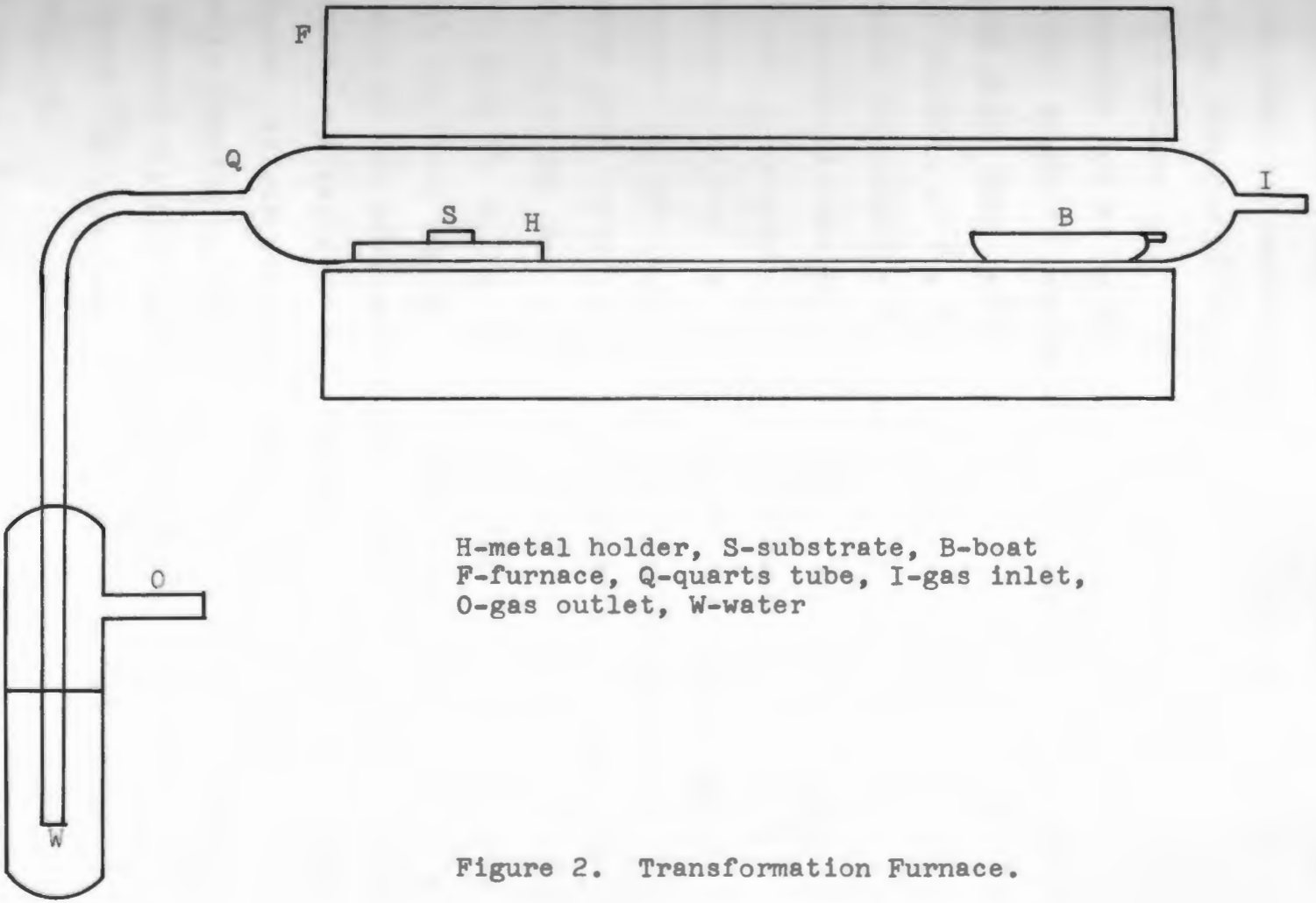

H-metal holder, S-substrate, B-boat
F-furnace, Q-quarts tube, I-gas inlet,
O-gas outlet, W-water

Figure 2. Transformation Furnace.

Fig. 3 is a photo-micrograph of a layer showing these crystals. In order to remove them, the layer is heated to 120°C in an oven for 48 hours.

Elemental samples:

Elemental silver sulfide sensors were prepared on 1" x 1/2" x 1/16" sapphire substrates. Attempts at making samples using glass substrates did not give reproducible dark or photo currents at low temperatures due to the relatively low thermal conductivity of glass.

Silver electrodes (Fig. 1-E) were evaporated over opposite ends of the layers to provide contacts for current measurements. Silver was chosen as the electrode material in an attempt to obtain ohmic contacts to the sample. A fine copper mesh (with holes 25 μm on a side) is placed between the layer and the silver source to absorb infrared radiation from the silver boat. This radiation would otherwise heat the layer enough to damage it.

Sample S6 was made using a different electrode geometry. This sample is a layer of Ag_2S sandwiched between two layers of aluminum. Silver electrodes were then deposited over the aluminum to provide contacts to the external circuit. Sample S8 had another electrode geometry. Two pointed electrodes of silver paint were applied to the layer approximately 2 mm apart (Fig. 9).

Vidicon targets:

The samples used as vidicon targets were prepared in much the same way as the elemental sensors. The differences

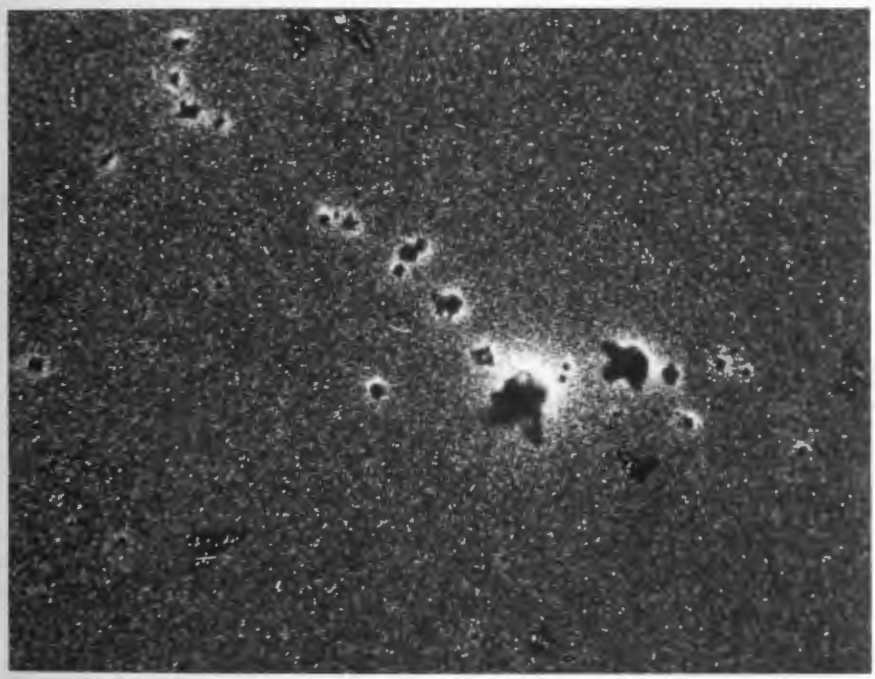

Figure 3. Ag_2S after transformation
(large crystal is 50 μm)

in preparation are noted here. The layers are deposited on glass substrates which have been previously coated with tin-oxide. The tin-oxide layer is a transparent conductor which acts as one electrode for the sample while the scanning electron beam completes the circuit. In addition to conventional continuous layers, island-type targets were also made. These targets are arrays of square islands of Ag_2S, 25 μm on a side, with the islands separated from each other by 5 μm. The targets were made by depositing the silver layer through a fine copper mesh which was in contact with the substrate. This mesh acted like a mask. Figure 4 is a photomicrograph of such a target.

Instrumentation:

Cryostat: In order to determine the mechanism which gives rise to the dark current, current versus temperature measurements were performed on several samples. These measurements were made in the temperature range 300 K to 100 K within a cryostat. The cryostat (Fig. 5) is an evacuated chamber which is used to control the sample temperature. While in the cryostat, the sample can either be kept in the dark or be illuminated through a glass port. A copper plate shields the sample to block the infrared radiation from the cryostat walls which are at room temperature. The radiation shield has a small hole drilled into it to allow light from a monochromator to illuminate the sample during photocurrent measurements. To keep the sample from warming by convection, the cryostat is pumped down to a pressure of

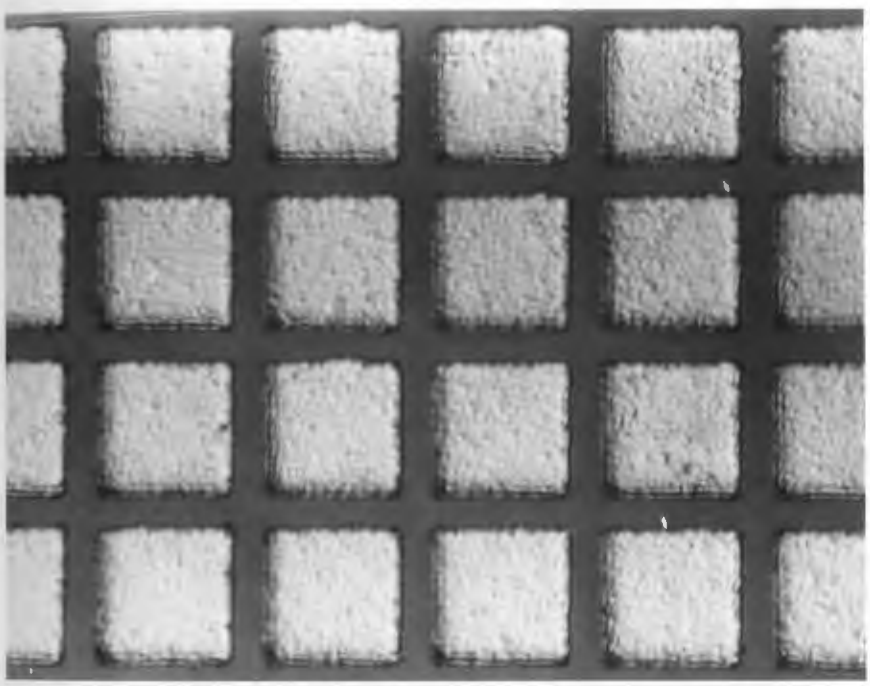

Figure 4. Photomicrograph of an Island Target (Islands are 25 μm)

E-electrode
C-cold finger
B-plexiglas
R-reservoir
T-thermocouple
F-feedthrough
S-sample
P-vacuum connection

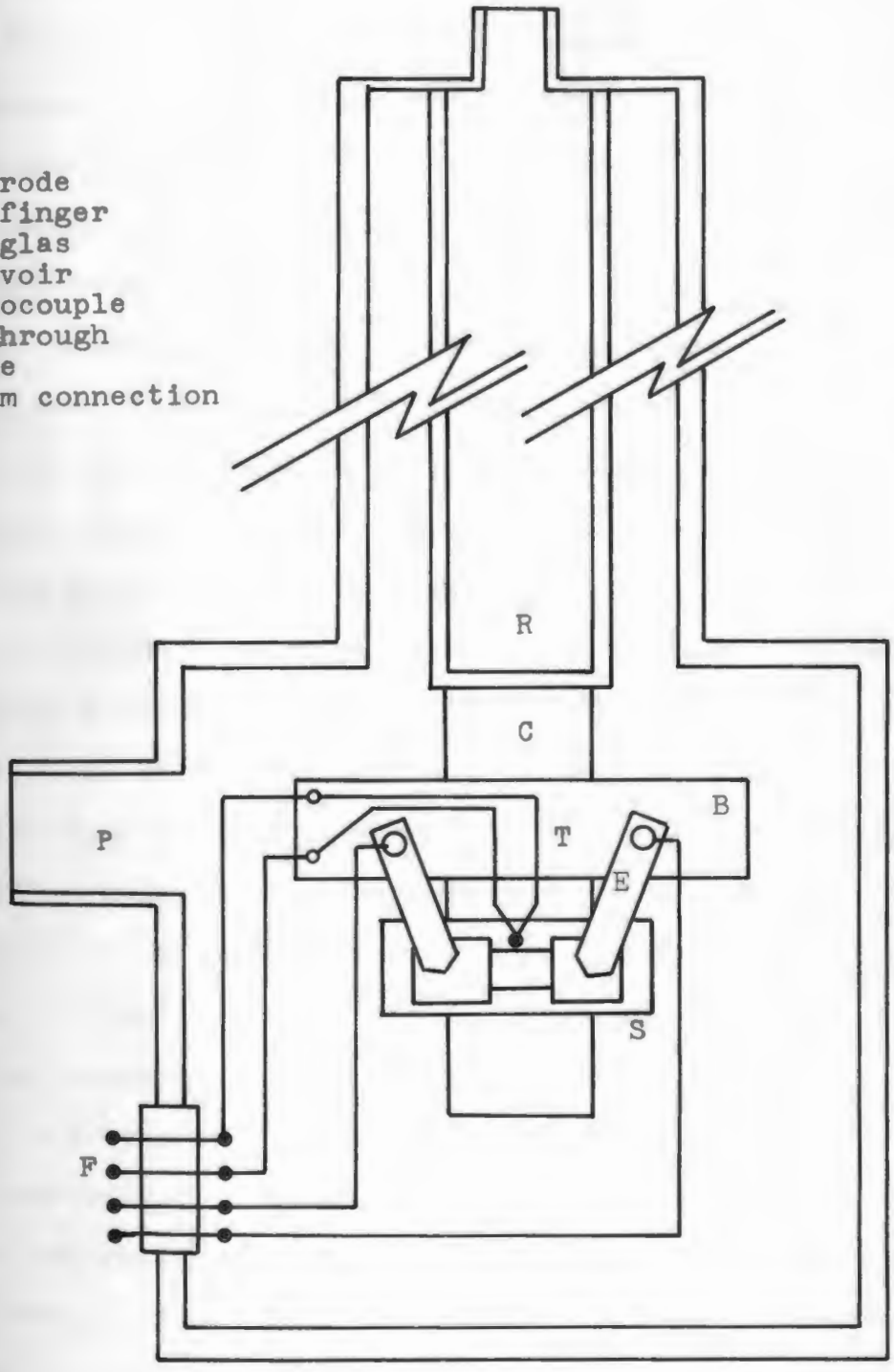

Figure 5. Cryostat

about 10^{-2} torr by a small diffusion pump. This pumping also removes most of the water vapor which would otherwise freeze on the sample and hinder measurements. The sample is held against the cryostat's cold finger (Fig. 5-C) by two spring electrodes (E). The sample temperature is lowered by pouring liquid nitrogen into the reservoir (R) which is connected to the cold finger. The sample temperature is monitored by a small (0.002" diameter) thermocouple (T) which is glued to the sapphire substrate with silver paint. Silver paint was used because it is a good heat conductor. The reference junction of the thermocouple (Fig. 6-J) is kept at $0^{o}C$ in an ice-water bath made from distilled water. A Kiethley 153 microvoltmeter (K) is used to measure the potential difference between the two thermocouple junctions. This voltage is then recorded on a HP 7100BR chart recorder (H).

Two experiments were performed to determine the ability of the thermocouple to track changes in temperature. In the first experiment the reference junction of the thermocouple was placed in the distilled ice-water bath and the other junction was placed in liquid nitrogen. The voltage measured (about 5.6 mV) was equal to the value given in standard tables of thermocouple voltages (within experimental error). The second experiment was performed using the dark current measuring setup. Since the dark current of the material is an exponential function of 1/T, changes in the sample temperature will result in significant changes in the dark current. This allows us to use the dark current as a relative

temperature indicator. When the sample was warmed and cooled rapidly, the dark current and thermocouple voltage rose and fell together, indicating that the thermocouple tracked the sample temperature accurately.

Sample current measurement:

The sample current measurement circuit consists of the following. A Krohn-Hite 5100A function generator (Fig. 6-G) provides a 13 Hz sine wave which is applied across a series combination of the sample and a 1.1 M Ω 1% sampling resistor (R). The voltage across this resistor is amplified by a Brower 261 preamplifier (P) and passed to a Brower 131 lock-in voltmeter (V). A synchronization pulse is supplied to the lock-in by the function generator. The lock-in is tuned to 13 Hz and its integration time constant was 0.1 sec. The output of the lock-in was recorded on the chart recorder (H) along with the thermocouple output.

A lock-in voltmeter was used because several researchers[4,5,6,10] have shown evidence of ionic conduction in Ag_2S. If a DC voltage is placed across a material which exhibits both electronic and ionic conduction, the ions will tend to form a space charge at one electrode. This charge polarization results in a decreasing electric field inside the material as the charges polarize. This causes the electronic current to decrease and it may mask out the effect one wishes to measure. AC measurements will eliminate this problem as described in the theoretical section.

When semiconductors are cooled from room temperature

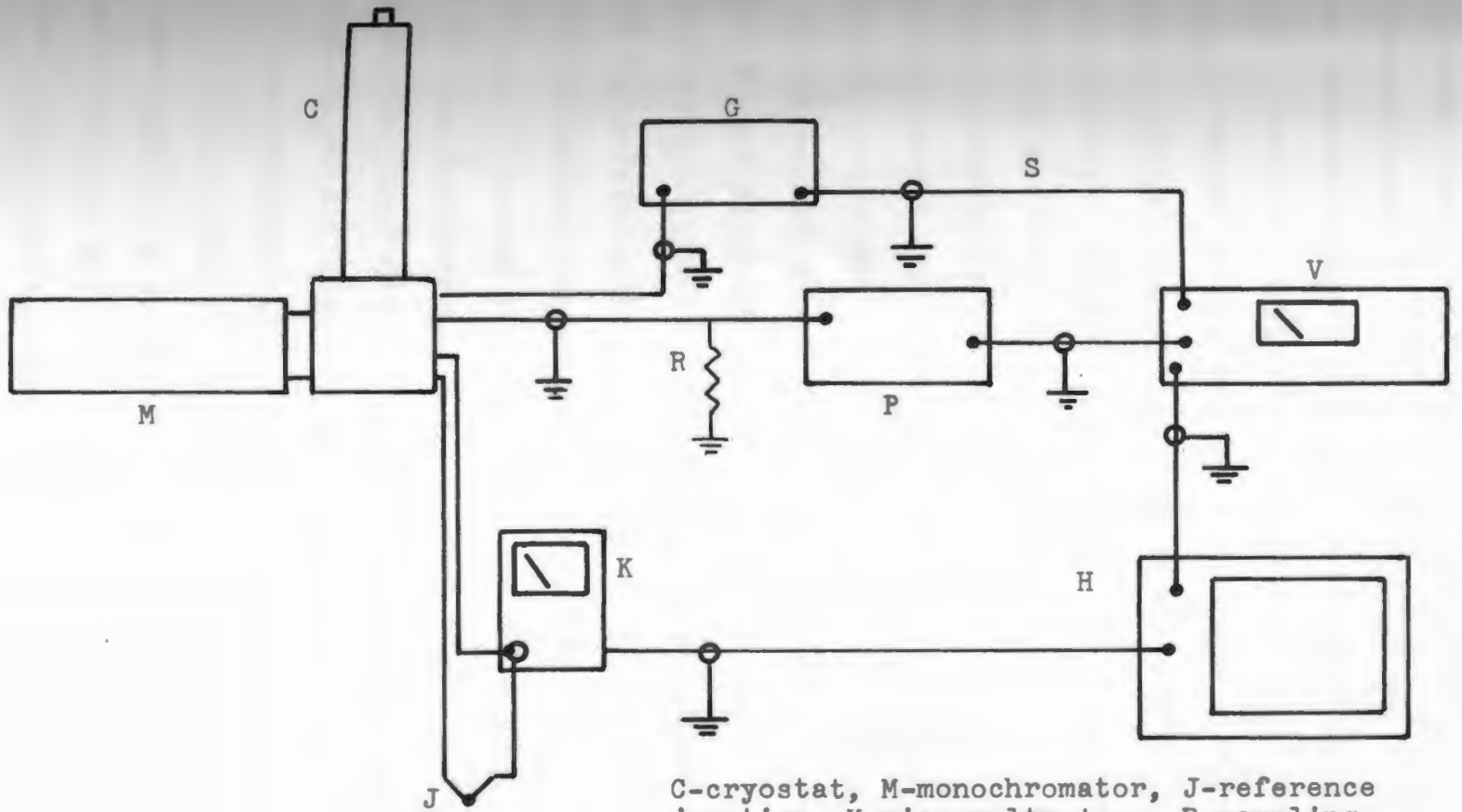

C-cryostat, M-monochromator, J-reference junction, K-microvoltmeter, R-sampling resistor, G-sine generator, P-preamplifier V-lock-in voltmeter, H-chart recorder, S-sync pulse line

Figure 6. Elemental circuit configuration

to liquid nitrogen temperatures, the resistivity may decrease by several orders of magnitude. Since there is usually stray capacitance associated with a circuit, one must be careful when measuring resistive effects that the resistive current does not become as small as the capacitive current or the latter will mask out the former. Fig. 7 is a phasor diagram of the resistive and capacitive currents in a sample at room temperature. Since the resistive current is so much larger than the capacitive current, the resultant phasor is approximately equal to the resistive phasor. When the sample is cooled and the resistivity drops by several orders of magnitude, the unchanged capacitive current will mask out the resistive current (Fig. 7-B). Note that the magnitude of the capacitive current is the same in both of the diagrams only the scale is changed. Since the capacitive impedance is inversely proportional to the frequency, selecting a low frequency will make the capacitive current smaller therefore making the above problem less severe. In order to further diminish the capacitive effect, a lock-in voltmeter is used. Since the lock-in is a phase sensitive instrument, it can be adjusted to measure a signal which is at a fixed phase angle from a reference signal.

The only critical adjustment necessary on the lock-in is the phase adjust. A crude adjustment was made at room temperature by maximizing the meter deflection since Fig. 7a indicates that the resistive current should dominate. The first dark current versus temperature data taken at this

crude adjustment indicated (after extrapolation of the data) that the dark current at 90 K would not be measurable due to the noise. Since the phase adjustment is critical at low temperatures (Fig. 7b), and since the dark current should be less than the noise, the phasing was fine tuned at 90 K to indicate zero current.

Light sources:

IR radiation for photocurrent measurements was provided by a Bausch and Lomb 33-86-03 single grating monochromator. This monochromator uses a tungsten lamp and a 675 groove/mm diffraction grating. The wavelength range emitted by this instrument is from 0.7 μm to 1.6 μm. A Corning 2-64 filter was used to block second order diffractions. The entrance and exit slits were both set to 6.0 mm which results in a dispersion of 125 A/mm. White light going into the monochromator could be blocked by a shutter. A second light source that was used was a tungsten lamp filtered with a polished germanium wafer to provide wavelengths greater than 1.8 μm. The power density in the sample plane for this source was 2.7 mW/cm^2. An Eppley thermopile was used to measure the radiant power density of both of the light sources.

Vidicon system:

The vidicon targets were analyzed in a demountable vacuum system which used a conventional vidicon camera tube. Vidicon is a generic name for a photoconductive camera tube. The vacuum system (Fig. 8) consists of a

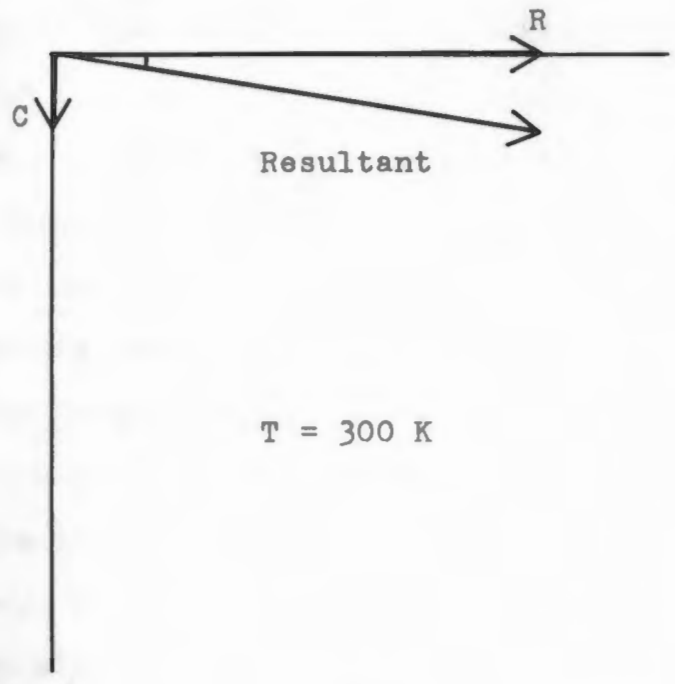

(a)

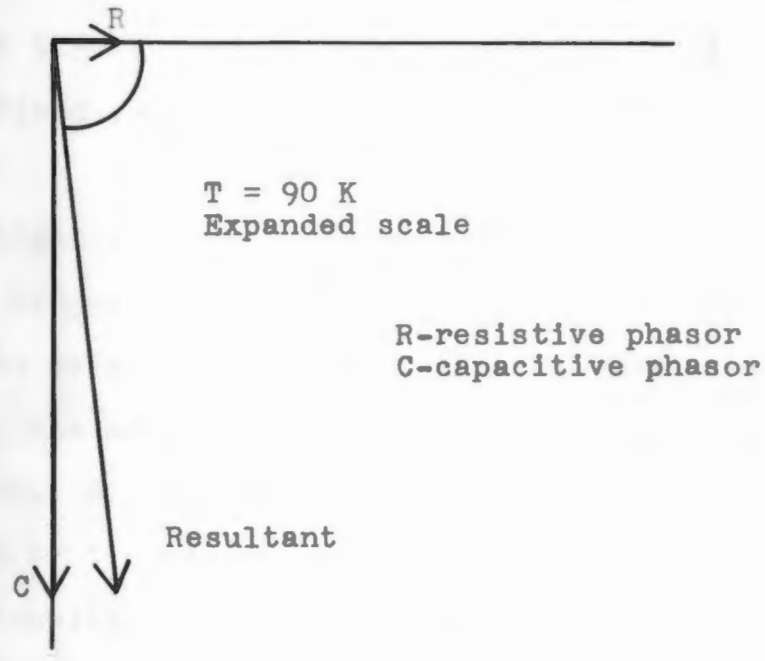

(b)

Figure 7. Phasor Diagrams

stainless steel tube which has ports to hold the vidicon gun, the target holder, the sapphire window, and the pumps. The system is pumped by a Vac-Sorb roughing pump and a Vac-Ion ionization pump to operating pressures of 10^{-8} torr. The electron gun (Fig. 8-G) and deflection coils (C) are mounted horizontally on one of the system ports. A sapphire window is mounted opposite the gum to allow light to fall on the target (T). The target and field mesh (M) are mounted on a cold finger which is attached to a removable vacuum fitting in such a way as to place the target between the gum and the sapphire window. There is a liquid nitrogen reservoir in this fitting to allow the target to be cooled. The target current is amplified by a 10 MHz preamplifier and a post amplifier before being displayed on a TV monitor. The camera is scanned using commercial broadcasting standards. These include a 525 TV line picture consisting of two interlaced picture fields, 1/30 sec frame rate, and a 3 to 4 aspect ratio.

Incident light is supplied by a tungsten lamp and a lens system to project a resolution test pattern transparency onto the target. The amount of light can be modified by placing one or more neutral density filters into the optical path. A polished silicon wafer (which transmits light with $\lambda > 1.2$ μm) can also be placed in the optical path. Optionally, the light can be chopped at 13 Hz.

Experiments Performed:

Elemental samples: Before any experiments could be

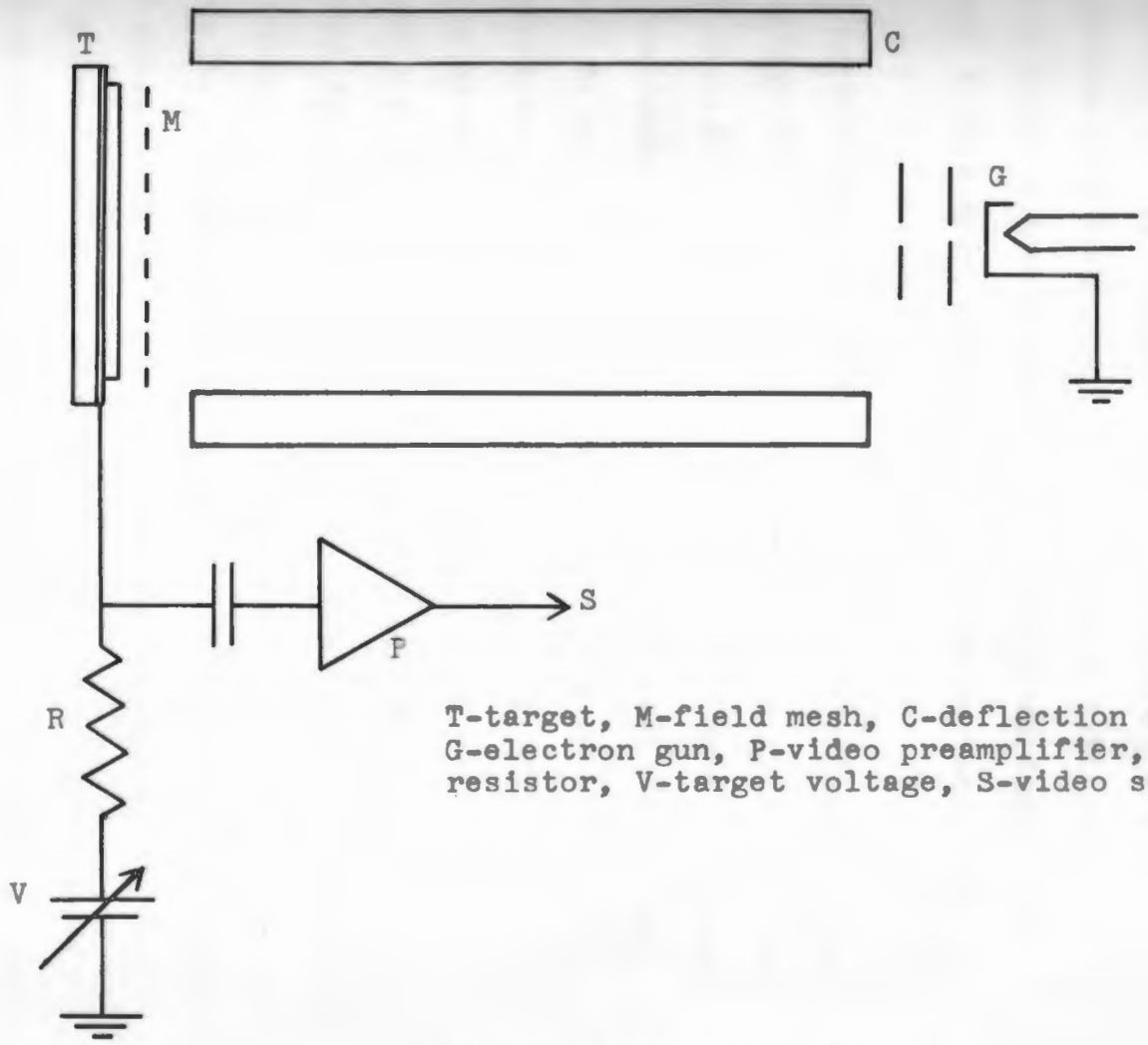

T-target, M-field mesh, C-deflection coils, G-electron gun, P-video preamplifier, R-load resistor, V-target voltage, S-video signal

Figure 8. Vidicon Schematic

performed, the sample contacts had to be tested to see if they were ohmic. A variable voltage was applied across the sample and the current was monitored. The sample current was recorded for ten values of voltage from zero to 50 mV. The polarity of the voltage was reversed and the experiment was repeated. In addition, the sample was placed on a Tektronix diode curve tracer. The maximum voltage swing was about 1 volt and the repetition frequency was about 1 kHz.

To detect ionic conductivity, sample S8 (Fig. 9) was examined under a microscope using a tungsten lamp for illumination. A variable DC power supply was applied across the two pointed electrodes and the voltage was slowly increased. At a voltage of 80 volts (a field of 40 volts/mm), photographs were taken. Several photographs were taken at intervals of about 15 seconds.

Dark current versus temperature measurements were made on several samples using an input voltage in the range 100 mV to 500 mV rms. Current values were taken every 5 kelvins from room temperature (300 K) to 90 K. At each temperature where a measurement was desired, the sample was slowly cooled by pouring small amounts of liquid nitrogen (about 5 cc) into the cryostat. The sample was cooled until it was slightly colder than the desired temperature, T, and the dark current was recorded at T. Then the sample was allowed to warm until the temperature was slightly higher than T and the dark current was again recorded as it passed

through T. More nitrogen was added to continue on to the next temperature point and the same procedure was followed. This entire procedure was repeated again as the sample warmed from 90 K to room temperature.

Photocurrent versus photon flux measurements were made using the same setup as above with the addition of the monochromator. At a temperature of 90 K and using a wavelength of 1.0 μm, photocurrent measurements were made as the intensity of the monochromator was varied in fixed steps. Inconel neutral density filters were placed in the optical path of the monochromator and the shutter was opened for a few seconds to allow the current to stabilize. Photocurrent values were taken as the photon flux was varied over three orders of magnitude. These data were used to normalize the spectral response curve.

Spectral response measurements were done at 90 K using the same setup as above. Photocurrent measurements were recorded from 0.7 μm to 1.6 μm at intervals of 0.1 μm. The monochromator shutter was opened for a few seconds to allow the photocurrent to stabilize, after which the shutter was closed. This procedure was followed starting at 0.7 μm and working up in wavelength. It was repeated in the other direction starting at 1.6 μm. After a week or two of experimentation, it was noticed that the response of the sample decreased. Re-heating the sample in the oven rejuvenated the sample.

An experiment to determine the effects of longer

wavelength radiation ($\lambda > 1.8$ m) on photocurrent was also performed. At 90 K, the photocurrent was first checked momentarily using a wavelength of 0.8 μm at a low power level (0.22 mW/cm^2). The long wavelength source (a tungsten lamp filtered by a germanium wafer) was turned on to flood the sample with long wavelength radiation and the photocurrent (at $\lambda = 0.8$ μm) was momentarily checked every few minutes.

Vidicon targets:

Mostly qualitative experiments were performed using the vidicon system. In order to determine the validity of the resolution measurements, the maximum resolution of the system had to be measured. To do this, the target was replaced by a zinc sulfide screen. By using a target voltage of 2 kV and by stopping the electron scan, the beam hits the zinc sulfide and causes a small spot to light up. The current was reduced to give the smallest spot possible. Using a microscope with a calibrated reticle, the minimum spot size, hence the resolution, was determined. Generally, the targets were tested for photoresponse at room temperature and 77 K. The response was maximized by adjusting the target voltage (Fig. 8-V). The maximum target resolution was determined by projecting the resolution test pattern onto the target and examining the TV monitor. The smallest lines that could be distinguished on the screen gave the resolution. The target sensitivity was measured by decreasing the light intensity to the point at which the image

was barely visible. An image fade-out effect was observed so the response was checked using chopped light to get a permanant image.

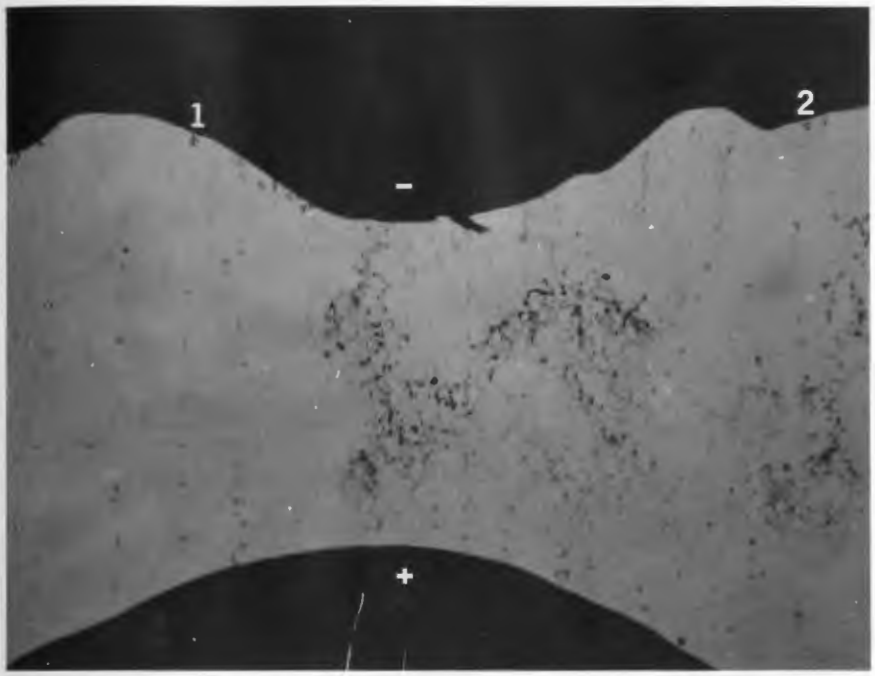

a

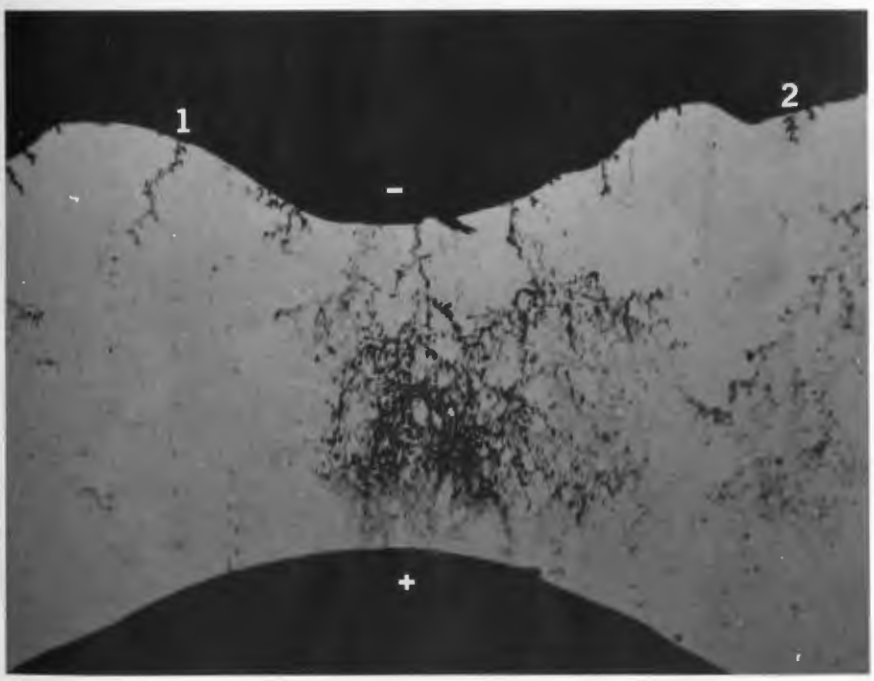

Figure 9. Silver tracks in thin layers (electrodes are 2 mm apart)

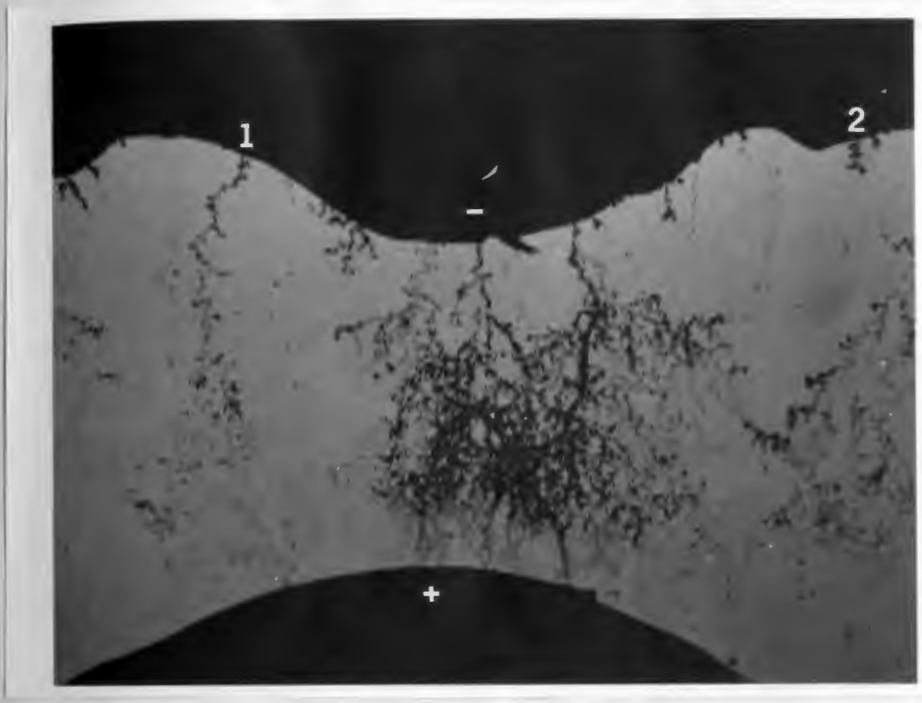

c

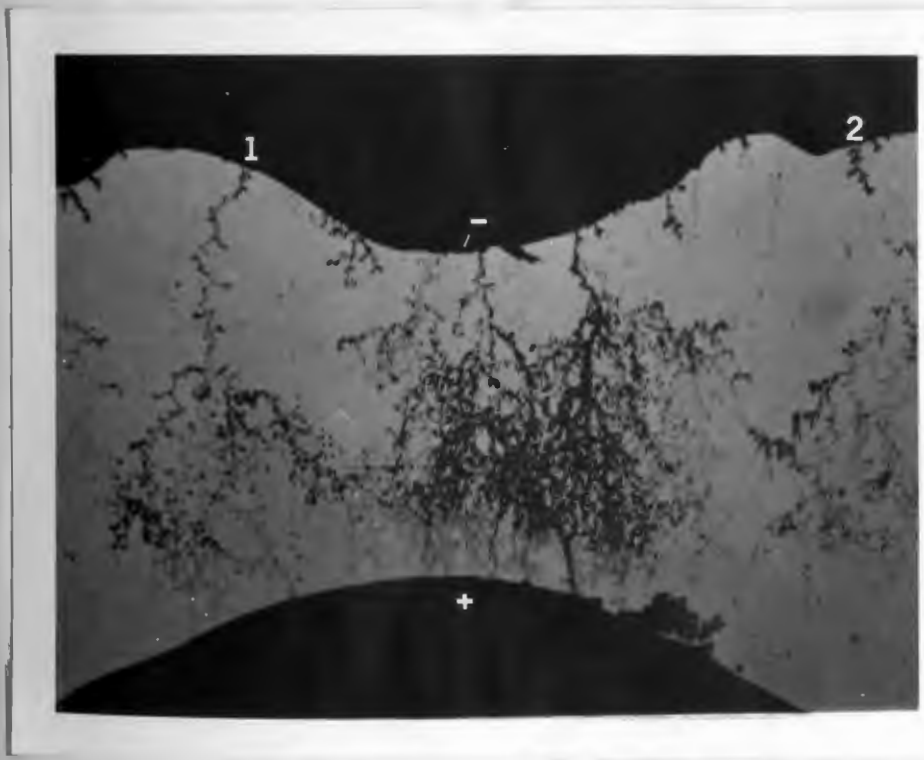

d

Figure 9. (continued).

III. RESULTS

Elemental Samples:

The results of the ohmic contact experiment are shown in Fig. 10. Since the current vs. voltage curve is a straight line through the origin, the contacts are indeed ohmic. When the sample was put on the diode curve tracer, a similar straight line through the origin resulted. Several researchers[4,5,6] have found the majority carriers for Ag_2S to be electrons. Our results are in agreement with this result on the basis of the simple experiment already described. In a circuit consisting of only the layer and an ammeter, there is no driving voltage, hence no current. Local heating near one electrode generates a concentration of free electrons. These electrons diffuse away from the heat source through the material. The direction of the resulting current shows that mainly negatively charged carriers (electrons) could have been generated from the heating.

A circuit consisting of a sample in series with the Kiethly microammeter was used to determine the sign of the majority carrier. A small heat source (a soldering iron) was placed on the substrate near one end of the sample. As the of the sample heated, the direction of the current through the sample was noted using the ammeter. It was found that the current direction was out of the heated electrode. This

would indicate that negatively charged particles (electrons) are the majority carriers.

The photomicrographs of the ionic conductivity experiment are shown in Fig. 9. The electrodes are marked as shown. Fig. 9-a shows sample S8 at the beginning of the experiment before the electric field was turned on. The dark patches are silver ions which have already become atoms. These appeared because the sample was exposed to a high intensity light level while the microscope was being focused. Points 1 and 2 show the start of the branching effect. The field at this time is about 40 volts/mm. In Figs. 9-b,c,d, the branches at many points continuously grow.

The dark current vs. temperature data for several samples are shown in Fig. 11. Each set of points was taken at a different voltage to cover the largest temperature range possible. The data points lie along a straight line when plotted on a semi-log scale. This indicates that the relationship between the dark current and temperature is of the form:

$$\ln(I/I_o) = -K/T$$

or

$$I = C \exp(-K/T) \qquad (16)$$

where K and C are constants. If we compare this relationship to eq. (5), K is of the form $E_r/2k$, and E_r is 0.66 eV as determined by the slope of the line.

The resistivity of samples S1, S2 and S4, as calculated from the geometry, voltage and current was found to

be about 10^5 Ω-cm at room temperature. The sandwich layer, S6, was noisy and gave values of resistivity which were unreproducible. Its resistivity was found to be several orders of magnitude higher than the other samples. The dark current vs. voltage for S1 is shown in Fig. 10. It is a straight line through the origin.

Photoresponse as a function of photon flux density is plotted in Fig. 12. The data are plotted on a log-log scale. Since they form a straight line, the form of the equation is:

$$\log I \propto \log H$$

or

$$I = KH^a \qquad (17)$$

where H is the photon flux density. The slope of the line gives the value of a, which is 1/2 (to within experimental errors). Therefore, the photoresponse is proportional to the square root of the photon flux.

The spectral response of S1 is shown in Fig. 13. In this figure, the steep drop around 1.2 μm is due to the absorption edge. Photons with a wavelength of 1.2 μm have an energy of 1.0 eV. At 90 K the lowest detectable illumination was 5 $\mu W/cm^2$ at a wavelength of 1.0 μm. No sample responded to wavelengths longer than 1.8 μm. It was observed that the samples responded poorly after a week or two in the cryostat. The response could be improved by heating at 120°C for a few hours.

Normalization of spectral response:

Since the photon flux density of the monochromator is

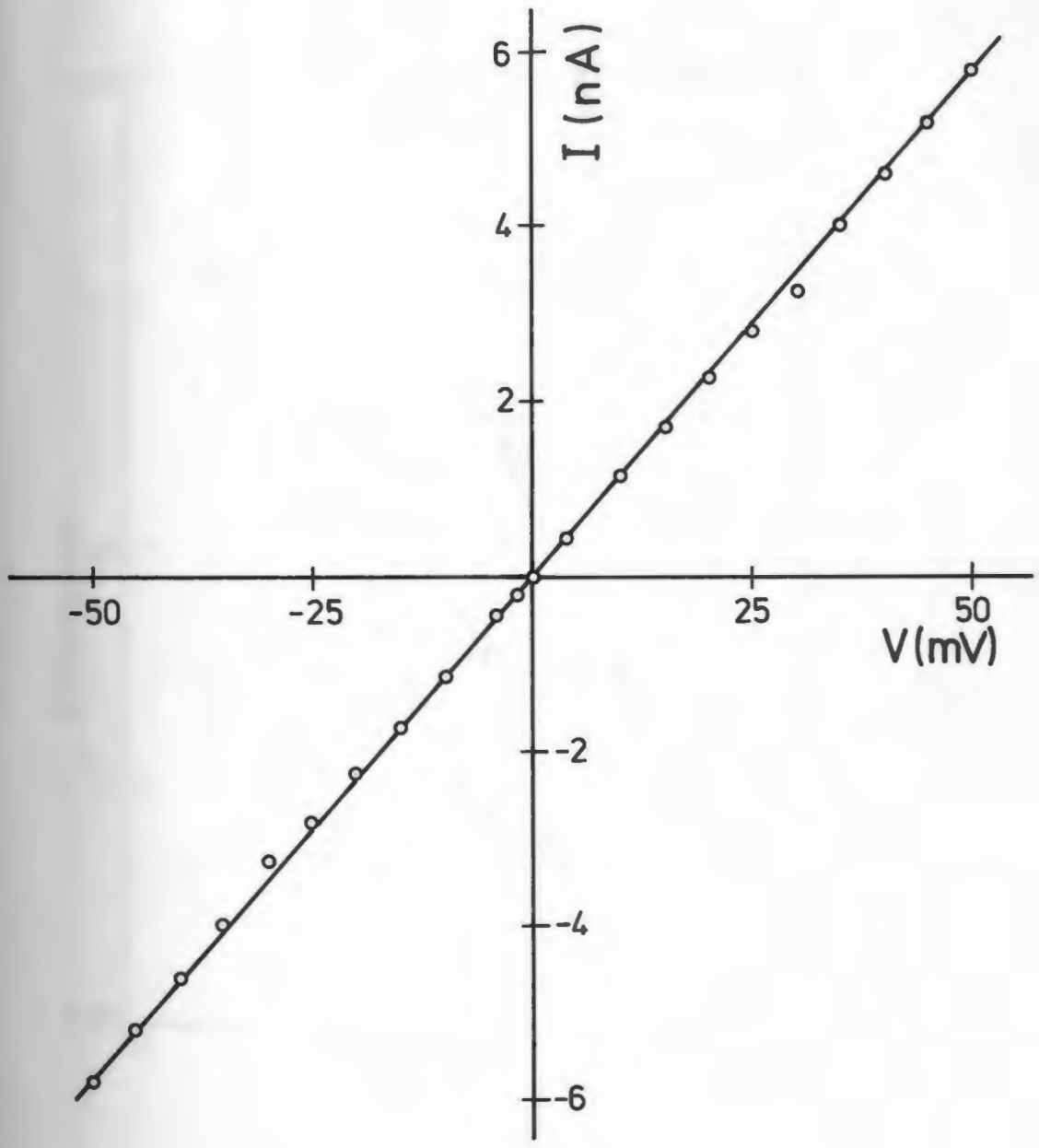

Figure 10. Dark Current vs. Voltage

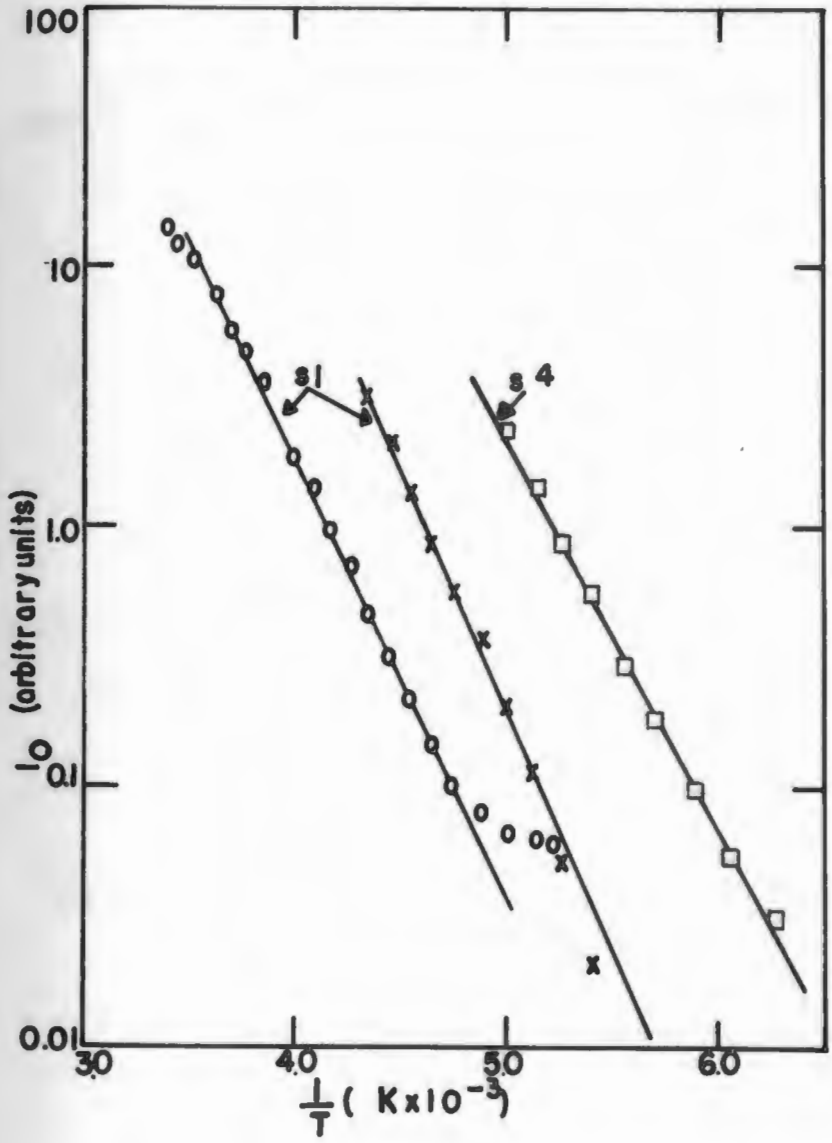

Figure 11. Dark Current vs. Temperature

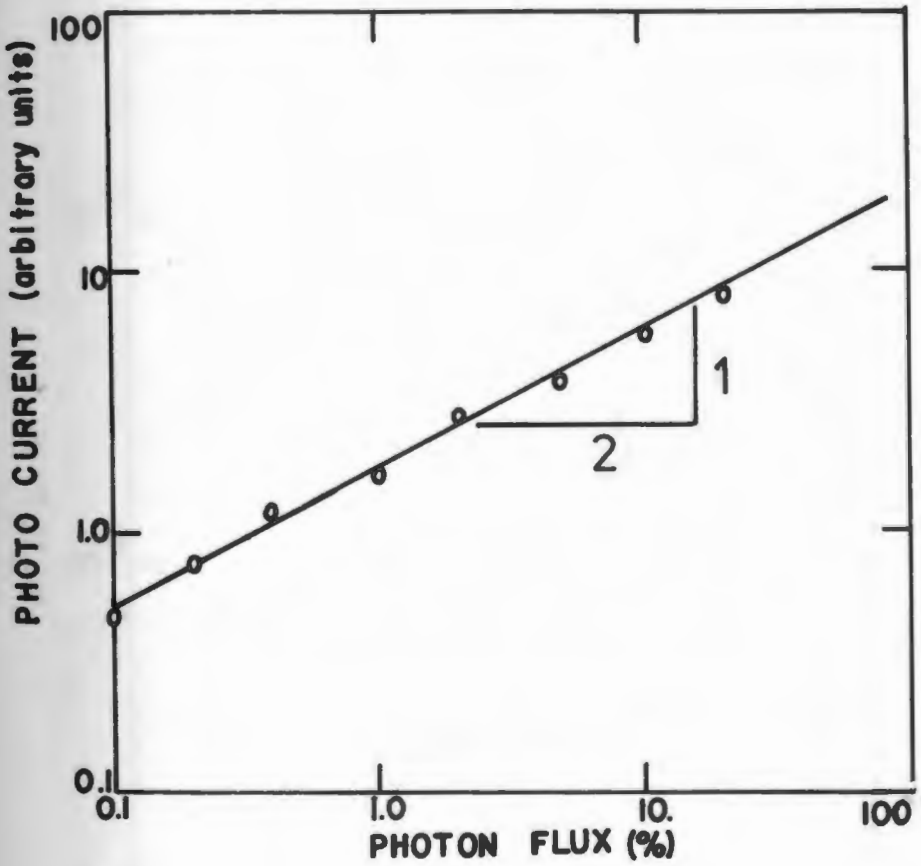

Figure 12. Response vs. Photon Flux

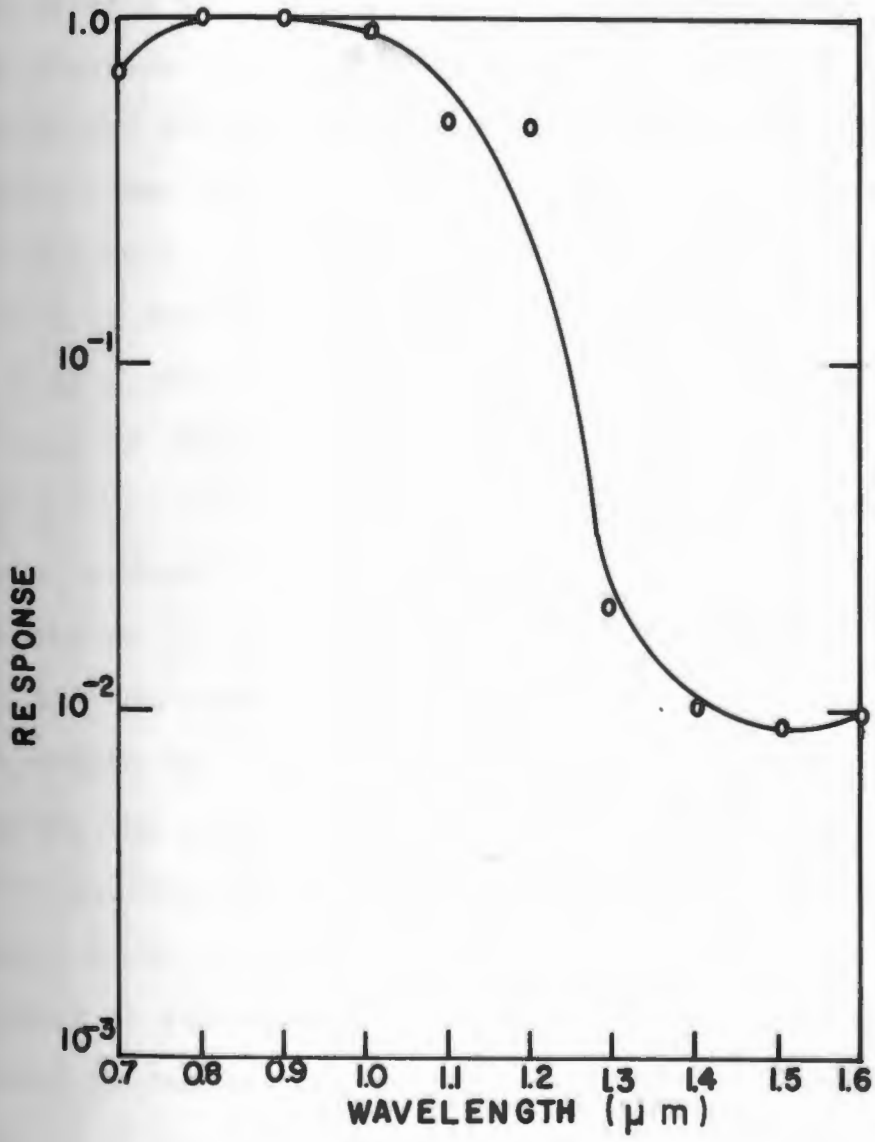

Figure 13. Spectral Response of Ag_2S

not the same at all wavelengths, the raw spectral response data must be corrected to reflect only the effect of the material. To do this, one needs the incident photom flux density as a function of wavelength and the sample response as a function of photon flux density. Using an Eppley thermopile, the monochromator was calibrated in terms of radiant power density (mW/cm^2) as a function of wavelength.

$$E = hc/\lambda \tag{18}$$

where E is the energy, c is the speed of light in vacuum, and h is Planck's constant. The power density was expressed in terms of joules/s^{-1}-cm^{-2} and the actual photon flux density was calculated at each wavelength used. The wavelength at which the sample gave the largest response was selected as the point of comparison for the normalization. That is, the relative response at 0.8 μm was set to 1.0. If a sample has a constant quantum efficiency at all wavelengths, the measured spectral response would only depend on the incident photon flux. Since the samples do not respond to all wavelengths equally, the normalized response is equal to the measured response (at a given flux density) divided by the percent response expected at that flux density.

The photocurrent vs. long wavelength ($\lambda > 1.8$ μm) flood time is shown in Fig. 14. If the data points lie along an exponential curve, the form of the equation is:

$$I = I_f - K \exp(-At) \tag{19}$$

To determine if it is exponential, the difference $I_f - I$ is

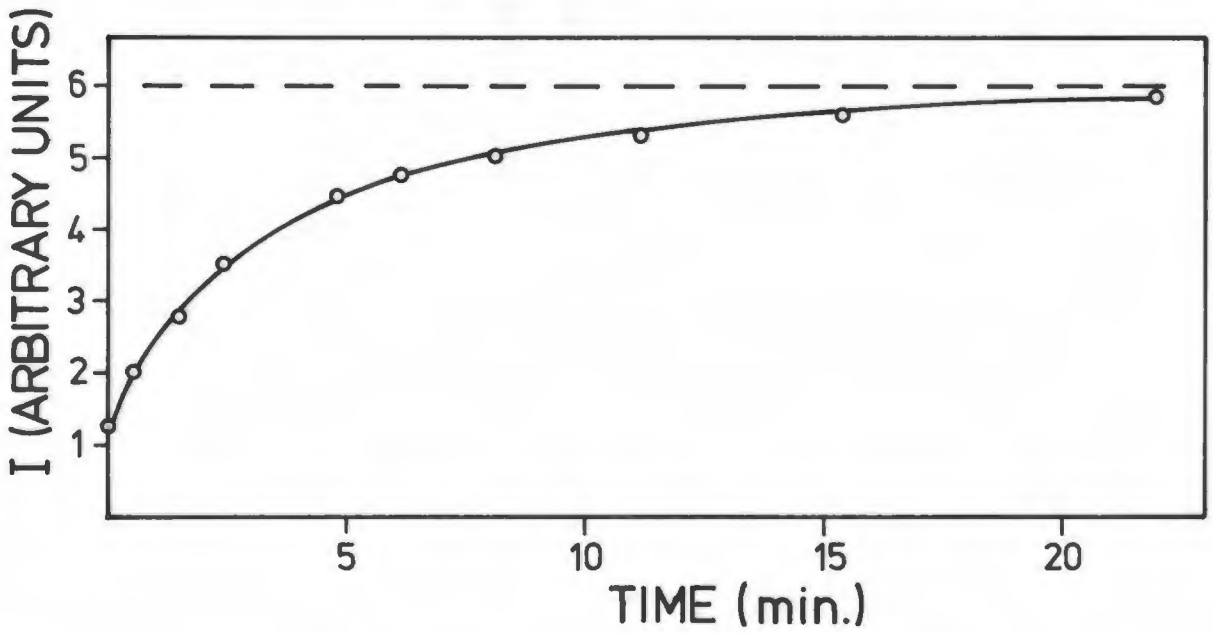

Figure 14. Photocurrent vs. IR Flood Time

plotted in Fig. 15. For the most part, it is a straight line when plotted as log $(I_f - I)$ vs. time. The form of this equation is:

$$\log (I_f - I) \alpha (-At)$$

or

$$I_f - I = K \exp(-At) \qquad (20)$$

Vidicon results:

As stated earlier, mostly qualitative measurements were performed with the vidicon system. It was found that the targets responded to light when cooled to liquid nitrogen temperature. Fig. 16 is a photograph of the TV monitor showing the response of target T20 to the transmission test pattern. The target temperature is about 77 K, the target voltage is 10 volts, and the incident radiant power density is about 100 $\mu W/cm^2$. Using the test pattern, the maximum resolution obtained with any target was about 10 lp/mm. However, the electron beam size was found to be 50 μm, which would allow for a limiting resolution of 10 lp/mm. This means the actual target resolution may be greater than 10 lp/mm. For this reason, the island targets did not improve the resolution. The intent was to limit the spreading of the incident beam due to the inter-island gaps.

The targets exhibited an image fade-out effect. When illuminated, the test pattern appeared on the TV monitor and slowly faded in about five seconds. The time for fade-out varied from one to ten seconds depending on the target. When the illumination was blocked, the image reappeared with

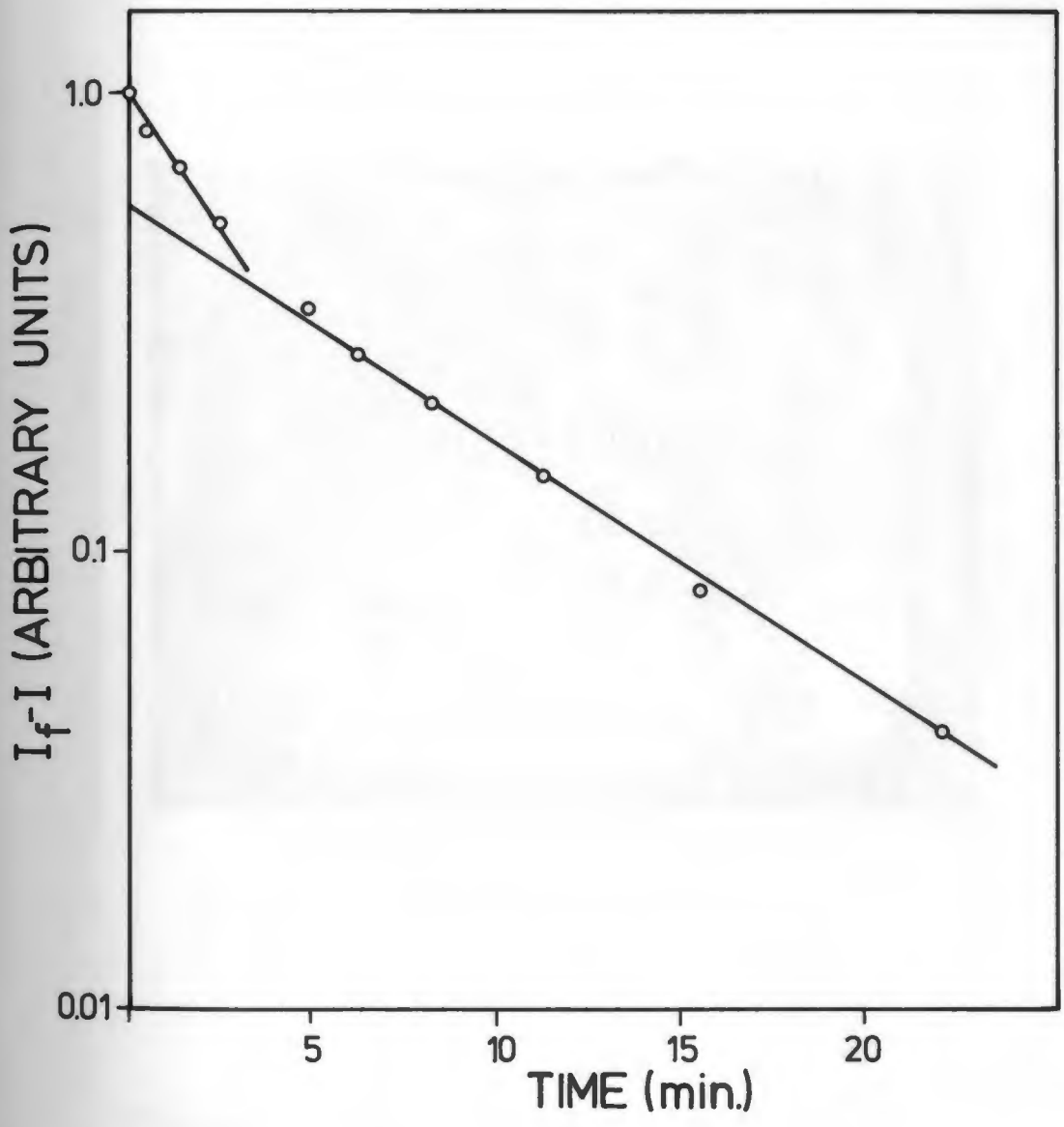

Figure 15. $I_f - I_{ph}$ vs. IR Flood Time

Figure 16. Image using Infrared Irradiation

reverse polarity (light where it was dark) and faded again. When using the chopper in the light path, the image could be sustained.

The targets would respond to low illumination levels (as low as 30 $\mu W/cm^2$) and some would respond to light filtered by a silicon wafer ($\lambda > 1.2$ m). However, the targets responded poorly after a few weeks in the system. It was also observed that if a bright image was projected onto the target for about five minutes, the target would retain the image in a silvery pattern. This burn-in (as it was called) could be removed and the degradation in response could be reversed by heating as with the elemental samples.

The vidicon targets showed a poor dynamic range as far as light intensity is concerned. This was probably due to the constant background illumination from the cathode. At operating temperatures, the cathode glows dull yellow. This probably provides enough stray light near the target to generate a considerable background.

IV. DISCUSSION

The verification of ohmic contacts to the sample is necessary before any other esperimental result can be discussed. The current vs. voltage curve (Fig. 10) and the results of the diode curve tracer experiment show that silver produced an ohmic contact to our Ag_2S layers. Silver was originally chosen because it seemed to be a logical choice since it is already part of the material. Mangalam, et al[5], suggest that silver did not make an ohmic contact in their experiments. Mangalam's experiment with Ag_2S was very similar to our work with the exception that she used chemically deposited layers. She states that evaporated silver electrodes did not make ohmic contacts to her layers. Mangalam tries to substantiate here claim with a theoretical discussion of work functions of the material and electrode. To give an ohmic contact to n-type semiconductors, the contact material should have a lower work function than the semiconductor. Mangalam states that the work function of Ag_2S is in the range of 3 to 4.8 eV. Since their work was done on chemically deposited layers, any number of impurities may have been present on the layer surface prior to the deposition of the electrodes. Bube[9] cites this impurity-barrier mechanism as a cause of non-ohmic contacts. The reason a non-ohmic contact forms is

due to a barrier between the material and the contact. This barrier can be eliminated by choosing an electrode material which will act as an impurity in the semiconductor and by applying the contact in such a way as to diffuse it into the semiconductor. Silver is contained in Ag_2S and the evaporation technique used tends to help the silver diffuse into the material. This is the probable cause of the ohmic contacts.

The photographs of the ionic conductivity experiment (Fig. 9) show the growth of some tree-like structure. Taking into consideration the existence of mobile silver ions[4,5,6,10], these branches are probably neutral silver. When the DC field is turned on, the ions migrate toward the negative electrode. When they reach it, they may capture a free electron and become silver atoms. Each new atom effectively extends the negative electrode into the material. The slightly increased field at these points (Fig. 9-a, points 1 and 2) draws more ions to it and the neutral silver forms tree-like structures. By examining the successive photographs in Fig. 9 the growth of branches 1 and 2 can be seen to extend as time progresses until some of the branches in the center region bridge across the sample and short it out.

It is plausible to assume that the degradation of both the elemental layers and the vidicon targets is due to the same effect which is described above but at a different rate. It will be shown that the silver ions are the recombination centers and that these centers play an important role in both the dark and photocurrents. If the ions are transformed

into silver atoms, the ion density decreases resulting in poor response. This occurs because the ions act as the valence band. It was observed that heating the samples improved the response. It is clear that the heating causes the silver atoms to recombine with the free sulfur which is in the layer. This increases the silver ion density.

Bube quotes the band gap of Ag_2S as 0.9 eV at room temperature. Since the dark current is usually due to thermal excitations from the valence band to the conduction band, the data shown in Fig. 11 could have been the result of band to band transitions. However, the results of the dark current measurements seem to indicate the existence of an energy level in the band gap 0.66 eV below the conduction band. Bube's value for the gap and my spectral measurements (as discussed later) eliminate the possibility that these data (in Fig. 11) were the result of band to band transitions. The linearity of the curve connecting the data points and the absence of a break in the curve indicates that these levels (recombination centers) are quite numerous. This is shown to be the case later in the discussion.

The calculated resistivity of several samples of the material, 10^5 Ω-cm at 300 K, is in agreement with work done by others[3,5]. The resistivity of S6, the sandwich layer, was calculated to be several orders of magnitude too high. We assume that there were contaminants on the layer prior to electrode deposition so the measurements taken from this sample were discarded.

The spectral response provides two important clues to the band structure. The first clue is the absorption edge at 1.2 μm. The sharp decrease in photocurrent for wavelengths greater than 1.2 μm results because the photons do not have enough energy to cause band to band transitions. Therefore, the band gap is equal to the energy associated with a photon whose wavelength is 1.2 μm. The calculated band gap is 1.0 eV at 90 K. This figure is slightly higher than Bube's figure of 0.9 eV at room temperature. This is due to the decrease in band gap as temperature increases. Bube quotes values for change in gap with temperature ($\Delta E_g/\Delta T$) for many semiconductors. He does not give a value for Ag_2S but all of the values he does give are in the range -10 to -100 meV/K. I assume, for rough calculations only, that $\Delta E_g/\Delta T$ is -5 meV/K for Ag_2S. For a change in temperature of 200 kelvins (100 K to 300 K), the decrease in band gap is 0.1 eV. Starting at 1.0 eV at 90 K, the calculated gap at 300 K is 0.9 eV. This is the figure given by Bube. The second clue taken from the spectral response concerns the region around 1.8 μm. The layers respond to wavelengths as high as 1.6 μm as determined by monochromator measurements. The long wavelength ($\lambda > 1.85$ μm) photocurrent test shows that the layers do not respond to wavelengths greater than 1.85 μm. This sharp drop in response implies that there is a second absorption edge between 1.6 μm and 1.85 μm. The response between 1.2 μm and 1.6 μm and the absorption edge near 1.8 μm would seem to be associated with

the recombination centers. Photons that are just energetic enough to excite electrons from the recombination centers (E_r = 0.66 eV) would have a wavelength of 1.82 μm. This agrees well with the explanation of the dark current and gives further evidence for the existence of the recombination centers.

Fig. 17 shows the spectral response measured at this laboratory (curve A) as compared with the data Mangalam[5] presents (curve M). Note that our data were taken at 90 K and Mangalam's was taken at 300 K. The general shape of the two curves is about the same. The absorption edge in Mangalam's work is about 1.4 μm. The calculated gap from this edge is 0.89 eV which agrees with both Bube's value and mine when it is corrected for room temperature.

Since the photocurrent depends on the square root of the photon flux (Fig. 12), the band structure of the material would seem to fit the one given in the theoretical section. Recall that this model basically requires a large number of occupied recombination centers and a set of shallow trap levels. The recombination centers have been found and it will be shown that the density of occupied centers is large. This points to the existence of shallow traps. This evidence only indirectly suggests the existence of traps. As to the identity of those states, Bube states that in the vast majority of cases, the origin of traps is unknown. He suggests surface states as the usual source of shallow traps.

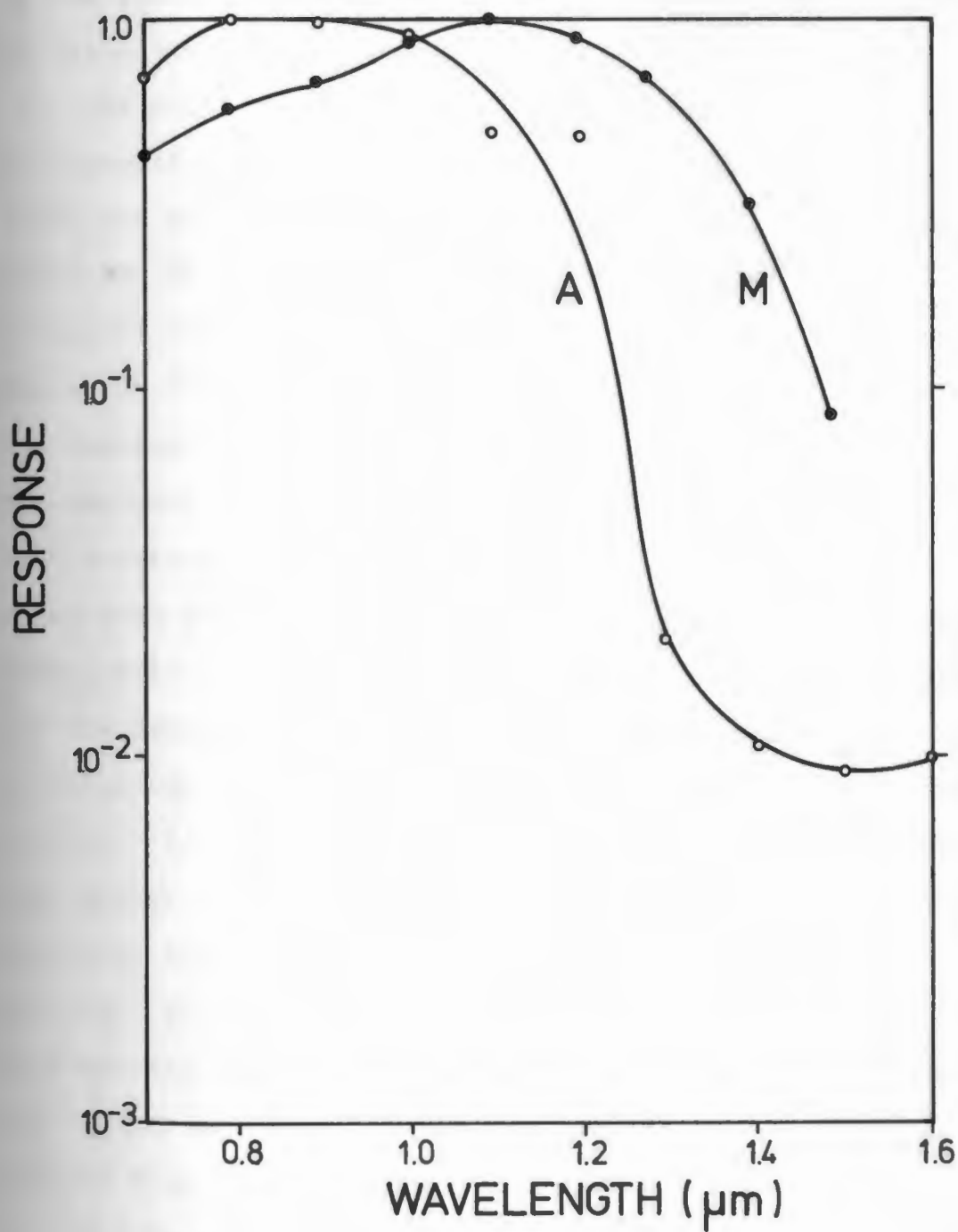

Figure 17. Comparison of Spectral Responses

Since the material is most likely a conglomerate of crystal groups, the traps may be associated with the irregularities in the structure. Fig. 18 shows the band diagram for Ag_2S as calculated from our measurements.

The photoconductivity of the material can be increased by absorption of infrared radiation ($\lambda > 1.85$ μm). Fig. 14 shows the increase in photocurrent as a function of time. Since the IR flood was constant, the time scale is proportional to the number of IR photons flooding the sample. Since the IR photons had wavelengths greater that 1.85 μm, the increase in photocurrent was not due to transitions into the conduction band from the valence band or the recombination centers. However, the IR photons could excite electrons from the valence band into the recombination centers. Recall that the photocurrent is proportional to the lifetime and the probability that an electron will fall into a recombination center is proportional to the density of unoccupied centers. If the recombination centers are slowly filled from the valence band, the lifetime of electrons in the conduction band will slowly increase, hence the slow increase in photocurrent. Bube[9] refers to this mechanism. Fig. 14 shows the photocurrent approaching a final value (I_f). At this value, all of the recombination centers are presumably filled. The data in Fig. 14 can be expressed as:

$$I = I_f - K \exp(-At) \tag{19}$$

To isolate the time varying part, eq. (19) is rewritten as

$$I_f - I = K \exp(-At) \tag{20}$$

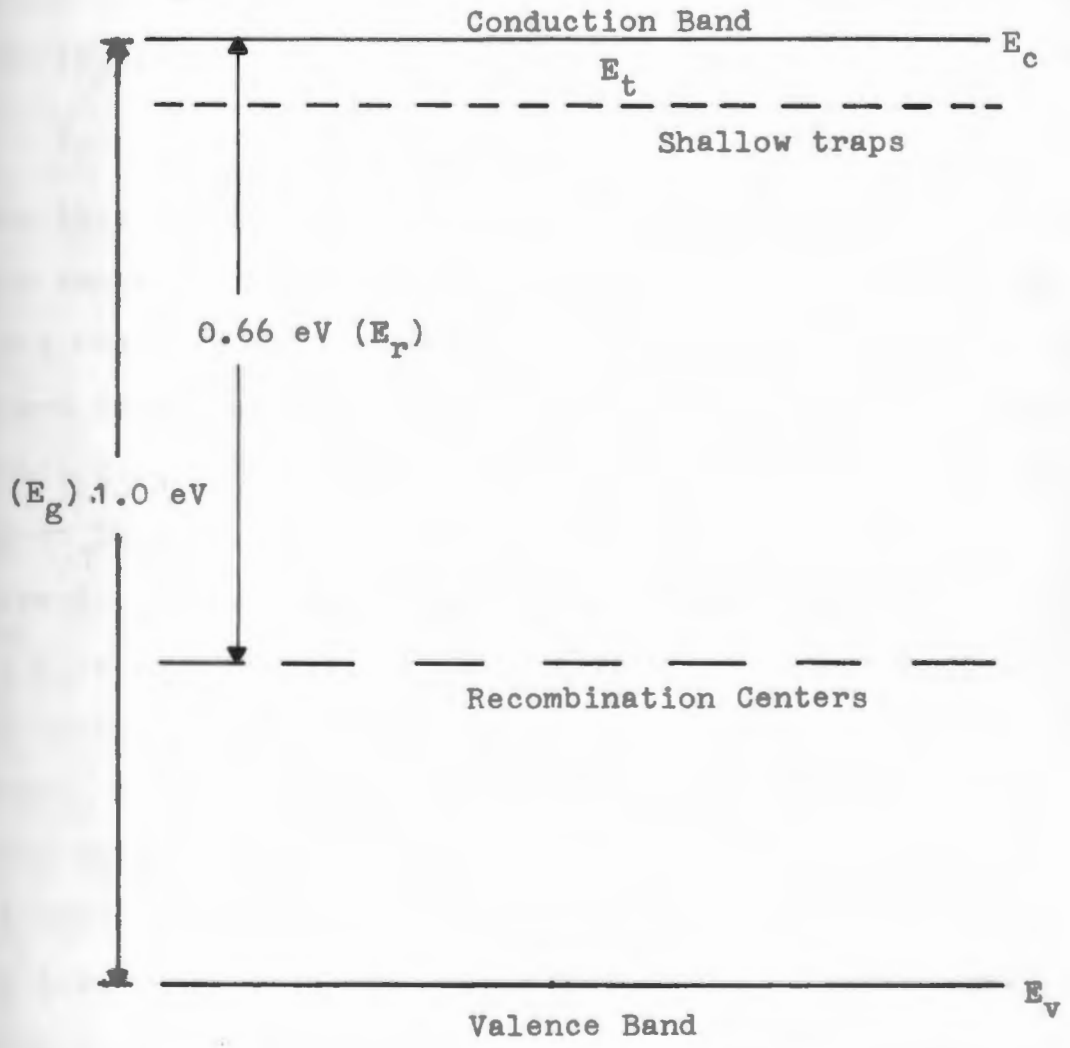

Figure 18. Energy Band Diagram of Ag_2S

Since the IR flux density is proportional to time, eq. (20) can be expressed as:

$$I_f - I = K \exp(-Bm) \tag{21}$$

where m is the number of IR photons that have been absorbed by the sample. Fig. 15 shows the data from Fig. 14 replotted in the form of eq. (21). The constant B contains the percent of photons absorbed (η) and the density of recombination centers (N_o).

$$I_f - I = K \exp(-\eta m/N_o) \tag{22}$$

From this equation we can determine the density of recombination centers. Since the final current (I_f) is about five times the initial current, it would seem that recombination occurs mainly at the recombination centers rather than by direct recombination. This is true because the trap filling due to IR absorption has a dramatic effect on the photocurrent. Since there is a large difference between I_o and I_f, η is probably large. η is likely to be in the order of 0.1 to 1.0. Isolated experiments have shown to be in this range. From Fig. 15, the value of N_o is about 10^{23} cm^{-3}. Since this value is in the order of the density of atoms in the material, it would seem that the recombination centers are associated with the silver ions. The break in the curve could be due to another set of levels near the recombination centers. These levels would have a larger capture cross section due to the steepness of the line. There are however not enough data points to positively prove the existence of this level.

The image fade out effect seen in the vidicon targets may have been the result of ionic polarization. Even at 77 K, the ions could still have sufficient mobility to move across the target whose thickness is about 0.7 μm. Where the target is illuminated, the ions may gain enough energy to drift with the DC field caused by the target voltage. Within a few seconds, they reach the end of the layer and polarize it, causing the image to fade away. When the light is removed, the ions can diffuse back into the layer causing a reverse current which in turn produces the reverse image which was observed on the TV monitor. This theory also explains the burn-in in some targets. As stated before, high illumination caused a silvery pattern to form on the target. In this case, sufficient numbers of ions were able to move to the end of the layer and transform into atoms. This seems to be the same process that produced the tree-like structures in Fig. 9. When the illumination was chopped, a fluctuating picture appeared on the TV monitor. Apparently the chopping frequency (13 Hz.) was high enough to keep the ions close to their original positions.

The island targets were made in an attempt to increase resolution. This structure was tried to reduce the lateral charge leakage across the target. If the material has a low resistivity, the scanning electron beam (which is 50 μm in diameter) will spread out when it hits the target. This spreading will increase the size of the smallest detail observable which reduces resolution. Since there was no

appreciable difference in resolution between the regular and island targets, lateral charge leakage is not a problem in cooled Ag_2S targets.

There are many opportunities for continued research on Ag_2S. Extension of dark current vs. temperature data to very low temperatures will reveal any structure near the conduction band including the shallow traps. The IR enhancement data presented here is incomplete. The enhancement could be studied using an infrared monochromator to produce narrow bands of IR as opposed to the broad band source we used. This would reveal the fine details of the level filling and show if there are any other levels near the recombination centers. Since there are varied reports concerning the work function, more study is needed here also.

There are many places for improvement in the vidicon system also. The targets should be prepared on sapphire substrates to improve cooling. The target should be shielded from the system walls as in the cryostat. The cathode presents a constant background which should be removed. To avoid the background, an off-axis electron gun could be used. In this system, the cathode is not in the line of sight of the target. The electron beam is turned by a magnetic field to strike the target. Since the resolution measurements were limited by the electron optics of the system, a finer electron beam could be used to determine the target resolution.

APPENDIX

NEAR INFRARED CAMERA TUBE STUDIES WITH AN Ag_2S TARGET *

H. Roehrig,** P. Aceto,
S. Mardix, P.M. McIlvaine,
and S. Nudelman**

---

* Presented at the 6th Symposium on Photoelectric Image Devices, Imperial College, London, September 1974. To be published in Advances in Electronics and Electron Physics.

** Now University of Arizona, Tucson, Arizona

NEAR INFRARED CAMERA TUBE STUDIES WITH AN Ag_2S TARGET

By: H. Roehrig*, P. Aceto,
S. Mardix, P.M. McIlvaine,
and S. Nudelman*
University of Rhode Island
Kingston, Rhode Island

I. INTRODUCTION

In recent years there has been a growing interest in chalcogenite photosensitive materials[1,2] One of their advantages is the response out into the near infrared region. Ag_2S for example has a peak response at 1.1 μm and falls off to a cut off at beyond 1.6 μm.[2] Its application for a near infrared TV-camera tube is therefore desirable.

The successful operation of a television camera tube of the vidicon type requires a sensing layer material which has high resistivity in order to provide charge storage.[3] High materials resistivity however seems to result in low quantum efficiencies.[4] In addition most photosensitive semiconductive materials - especially those sensitive in the near infrared and far infrared regions have a rather low resistivity.[5] Veith suggested that low resistivity materials still can be used in a television tube with a direct reading scanning electron beam.[6] This type of a camera tube he called "conductron."

This paper describes experiments done in a demountable camera tube using cooled and uncooled Ag_2S. The operational characteris-

---

*Now University of Arizona, Tucson, Arizona

tics suggest that there is a "conductron" effect combined with some charge storage.

II. VIDICON VERSUS CONDUCTRON

Before going into the description of the experiments, it seems worthwhile to point out the differences between a "vidicon" and a "conductron." Figure 1.a. shows the schematics of a vidicon.

The essential parts are the picture element or pixel (which consists of a resistor R_e and a capacitor C_e in parallel), the beam resistor R_b and the load resistor R_a. As the electron beam successively switches from one element to the next one, it charges each capacitor C_e to a certain value Q_o. Upon illumination the resistor element decreases its resistance and consequently the capacitor discharges by an amount proportional to the illumination within a frametime t_f.

The electron beam returns after a frametime and recharges the capacitor C_e by the amount of the previous discharge. During the charging period t_d a charge Q is deposited generating a current flow, which is the signal:

$$I = \frac{Q}{t_d}$$

$$Q = \int_o^{t_f} e \times J \times \eta \times a_e \times dt$$

Here t_f = frame time; J = photon flux; η = quantum efficiency; a_e = area of pixel; e = electronic charge.

One can see that the signal is proportional to the irradiation integrated over the frametime. Two important requirements on tube design are:

1. That the resistivity of the sensing layer material is in the order of 10^{12} Ω cm in order to have an optimum signal within a frametime of 1/30 sec.

2. That the beam resistance R_b is sufficiently small to permit optimum charging of the capacitor C_e in the dwelltime t_d which means $R_b C_e \ll t_d$.

The operational characteristics of a conductron are different from that of a vidicon as can be seen in Fig. 1.b. Here a picture element consists essentially only of a resistor R_e, and the target capacitance is minimal. The current which flows while the picture element is connected to the scanning electron beam is determined by the value of the resistor R_e during that time -- provided the beam resistance R_b and load resistor R_a are appreciably less than R_e. Optimum power transfer from picture element R_e to the resistor R_a requires that $R_e = R_a$.

$$I = \frac{V_T}{R_e + R_b + R_a} \simeq \frac{V_T}{R_e + R_a}$$

$$R_e \simeq \frac{V_T \times T_r}{e \times J \times \eta \times a_e \times \tau}$$

Here V_T = Target voltage; T_r = transit time of the electrons; e = electronic charge; J = photon flux; η = quantum efficiency; a_e = area of pixel; τ = lifetime of the electrons.

This requirement basically fixes the target resistivity. Assuming a maximum electron beam of 1 μA the minimum beam resistance is in the

order of 10^6 Ω. Assuming a typical element size on the target of 2.5×10^{-5} cm^{-2}, (which would correspond to a spatial resolution of 10 lp/mm) and a layer thickness of 20 μm, the picture element resistance would be around 8×10^6 Ω for a materials resistivity of 10^5 Ω cm. This seems to be the lower limit of resistivities useful for such a tube.

Figure 1.b. also shows in a dotted line the often unavoidable target capacitance C_e. This capacitance however is not desirable here and serves only to decrease the signal amplitude.

Knoll and Schroeder[7] in 1937 and Theile[8] in 1938 reported on the successful operation of such a "resistance-controlled" camera tube. In view of the poor photo-response of their sensing material, which was Cu_2O, they had to rely on a gain from a secondary electron emission process. Theile describes in great detail the operational characteristics and finds close agreement between theory and experiment.

One of the disadvantages recognized at first glance is the fact that in this kind of a resistance-controlled tube the signal is not proportional to the integration time t_f and it seems that, compared to a vidicon, the signal should be almost 5 orders of magnitude smaller.

In 1950, Veith described the "Conductron," as a desirable tube configuration[6]. He estimated that the signal would not have to be 5 orders of magnitude smaller than that of a vidicon. Rather it could easily be comparable. While the vidicon performs an integration on account of the high R_eC_e (time constant of the picture

element), the conductron might find an equivalence in long lifetimes of the electrons generated by the photon to electron processes in the sensing layer.

III. EXPERIMENTAL SETUP

One of the materials with low resistivity investigated was Ag_2S. It was known that it is photosensitive, with the sensitivity peaking at around 1.1 μm and then falling off to a cutoff at around 1.6 μm. Its resistivity was known to be in order of 10^5 Ω cm. In addition it can be increased to 10^7 or 10^8 Ω cm by liquid nitrogen cooling.

The Ag_2S-layers or targets were prepared by a three-step process.

In the first step of the process, microcrystallites of silver sulfide in the β-form are produced by a low temperature cristallization from a reactive solution. We used thioacetamide which reacts in an aqueous solution with silver nitrate preferably at 0 - 5 C. These micro-crystallites then served as nucleation centers for an overgrowth in the second step of the process until the crystallite size was about 1 - 10 μm. This overgrowth was accomplished by adding to the suspension of microcrystallites a source of inorganic sulfide, for example hydrogen sulfide or sodium sulfide. In the final step, the sulfide crystals from the second step were bound using epoxy resin as the binder to a transparent and conductive surface, such as glass which has previously been coated with a transparent conductive material thereby completing the photoconductive element or target.

Measurements were made in a demountable all magnetic camera tube, using a standard vidicon gun with an oxide coated cathode. Maximum target currents were in the order of 10^{-6} A. The corresponding mini-

mum beam impedances were in the order of 10^6 ohms as obtained from beam acceptance curves using metal targets. In general, the raster consisted of a square of roughly .72 cm^2 area.

The target was not shielded against radiation coming from the filament or the cathode, and only once was this felt to be a problem. In general, the levels of irradiation necessary to measure a photoresponse were higher than those due to the cathode and filament radiation. The target was connected to a liquid nitrogen dewar such that the target could be cooled. This was felt to be necessary for most of the targets in order to increase their resistivities to a point where the pixel resistance was higher than the beam impedance.

Dark currents and photocurrents were measured in two ways:

(a) With the sweep circuits disabled, the beam was directed onto the target element of interest. The D.C. current was measured as a function of the target voltage. This is what is referred to below as "non scanning".

(b) With the sweep circuits operating in normal mode, the average current was measured as a function of the target voltage. This is what is referred to below as "scanning".

IV. RESULTS

Figure 2 is a dark current versus target voltage plot for typical Ag_2S targets at room temperature (Curve I) and liquid Nitrogen temperature (Curve II) for scanning and non scanning. The photocurrent at 77 K as a function of the target voltage is also given (Curve III). In addition Fig. 2 shows a plot of the target current versus target voltage for a gold target (Curve IV).

The curves show the following:

There is hardly any difference between scanning and nonscanning, and this holds for dark currents as well as for photocurrents. There were also targets in which we noted differences between scanning and non scanning, but then this difference was at the most 1 order of magnitude and concerned mostly the dark current.

We calculated the beam resistance from the slope of Curve IV to be 1.6×10^{7} Ω (this was at 2×10^{-8} A beam current). The slopes of curves I and II then permitted calculation of the values of the Ag_2S resistivities at room temperature and liquid nitrogen temperature. The values are 1.6×10^{6} Ω cm and 5.7×10^{7} Ω cm. This was done assuming a pixel size of 50 μm in diameter and a target thickness of 10 μm.

It should be noted here that none of the calculations consider secondary electron emission, its change with temperature or contact potential. The electrical circuit considered is a simplified one and consists of a battery, a vacuum diode representing the electron beam, and an external resistor representing the target element addressed by the electron beam just as indicated in Fig. 1.b. In view of the simplifications, the data should not be considered very accurate.

The photocurrent at 77 K is almost 3 times higher than the dark current at 77 K. It was measured under irradiation with about 4×10^{16} photons/cm^2 sec. (Compare III with II)

At room temperature there was hardly any photocurrent noticeable. Even though it was there. Only a few targets showed an appreciable photocurrent at room temperature, and for those cases their dark current at

room temperature was lower than for most other targets.

The photocurrent-voltage curve is practically the same as the dark-current voltage curve. Both curves are almost linear and have practically the same slope.

We also checked the linearity of response. As one can see from Fig. 3, the γ depends somewhat on the target voltage and on the spectral composition of the illumination. In the average the value for γ is about .4.

Figure 4, curve I shows a typical spectral response curve, obtained with Ag_2S at 77 K. It was measured using a Bausch and Lomb Monochromator with a grating of 675 grooves/mm and a Tungsten filament. The data were corrected for $\gamma = .4$ and a power density of 76 $\frac{\mu W}{cm^2}$ per unit wavelength. The scanned area on the target was .72 cm^2. The quantum efficiency under these conditions was found to be $\eta_{(.72)} = .08$ % at 1.1 μm.

Figure 4, curve II shows in qualitative comparison a spectral response curve obtained by Mangalam et al.[2] There is very little difference in the position of the peak, which is about 1.1 μm, and the shapes of the two curves agree reasonably well.

Figure 5 shows a spectral transmission curve for an Ag_2S target. In good agreement with the response curve the transmission is low at below 1.1 μm and increases for longer wavelengths.

The spatial resolution was measured using a resolution power test target (USAF 1951) and was found to be about 9 ℓp/mm. As our targets showed spatial non-uniformities, this value of resolution is an average one.

Figure 6 gives an impression of the imaging of the test target. The picture was taken while the target was operated at first cross over. One of the problems of the uniformity is definitely the epoxy binder. This binder has been eliminated recently.

V. DISCUSSION

The important feature of the curves in Fig. 2 is the fact that there is hardly any difference between the scanning and the non-scanning mode. This demonstrates that the currents are determined mostly by the target element resistor, while the electron beam dwells on this particular target element. This is the typical conductron mode of operation. As described above this mode of operation is most efficient when the beam resistance is small compared to the target element resistance. This is verified in Fig. 2. The beam resistance at 20×10^{-9} A is about 2×10^{7} ohms. The target element resistance of the Ag_2S target at room temperature is about 6×10^{7} ohms. The photoresponse at room temperature is hardly noticeable. However, after cooling to 77 K the target element resistance has increased to about 2×10^{9} ohms. Now the photoresponse is very strong.

As indicated above some targets showed a substantial difference between scanning and non scanning. This apparently was due to the presence of a high capacitance in the target circuit, giving rise to some RC-storage effects. This excess capacitance might be traced to the special way of the target preparation. It probably results from poor thickness control of the layer of epoxy.

The data plotted in Fig. 4 shows a rather remarkable response of the material. Even though the material has a low resistivity such

that there are no or only very small RC-related storage effects, the response is not very much smaller than the response of materials operated in the storage mode e.g. PbO/PbS. For this photosensor, Hori et al.[9] obtained responsivities of 2×10^{-2} $\frac{\mu A}{\mu W/cm^2}$ at 1.1 μm wavelength. Thus, Ag_2S compares well with its response at 1.1 μm. Furthermore for the standard vidicon raster of 1.21 cm^2 whose value at 1.1 μm is about 3×10^{-4} $\frac{\mu A}{\mu W/cm^2}$, the difference is much smaller than the difference of 5 orders of magnitude expected from the lack of charge storage.

An important feature of Ag_2S is its spectral response. Even though the peak response is at 1.1 μm there is still an appreciable response at 1.6 μm This spectral region is of importance since the atmosphere is very transmittant at 1.6 μm - under special atmospheric conditions even much more transmittant than in the visible region at around .5 μm. This sensor gives imaging systems operating in the 1.6 μm window an appreciable range.

In conclusion, we feel that materials with resistivities in the order of 10^7 ohms cm can be successfully used in TV pickup tubes with a satisfactory response. In particular the data suggest that Ag_2S is a useful sensor material for the near infrared region.

ACKNOWLEDGEMENT: This work was sponsored by the U.S. Army Electronics Command, Fort Monmouth, N. J. through Night Vision Laboratories, Fort Belvoir, Va. under Contract No. DAAB07-69-C-0420, Project Themis.

REFERENCES

1. Kinoshita, A., Japan. J. Appl. Phys. 13, 1027 (1974).
2. Mangalam, M.J. et al., Indian J. Pure Appl. Phys. 7, 628 (1969).
3. Weimer, P.K., Forgue, S.V., and Goodrich, R.R., RCA Rev. 12, 306 (1951).
4. Redington, R.W., J. Appl. Phys. 29, 189 (1958).
5. Gebel, R.K.H., In "Ad. E.E.P." Vol. 22A, 189 (1966).
6. Veith, M.W., Le Vide 30, 887 (1950).
7. Knoll, M. and Schroeter, F., Phys. Z. 38, 330 (1937).
8. Theile, R., Die Telefunkenroehre 13, 90 (1938).
9. Hori, H., Tsuji, S., and Kiuchi, Y., In "Ad. E.E.P." Vol. 28A, 252 (1969).

DISCUSSION

J.D. McGee: Was there any ill effect on the thermionic gun cathode due to sulphur from the Ag_2S target?

H. Roehrig: We did not notice any ill effect on the thermionic gun cathode due to sulphur from the Ag_2S target. However, it is quite possible that any such effect was overshadowed by the fact that we operated in a demountable system, the frequent openings of which resulted in a rather short lifetime of the thermionic cathodes.

LEGENDS TO FIGURES

Fig. 1

Fig. 1 Schematics of a vidicon and a conductron.

Fig. 2

Fig. 2 Current-voltage characteristics (beam acceptance curves), scanning and non scanning.

I. Dark current versus target voltage for a typical Ag_2S target at room temperature.

II. Dark current versus target voltage for a typical Ag_2S target at 77 K.

III. Photocurrent versus target voltage for a typical Ag_2S target at 77 K.

IV. Target current versus target voltage for a gold target.

Fig. 3

Fig. 3 Linearity of response of a typical Ag_2S target for different target voltage and different spectral composition of the irradiation.

Fig. 4

Fig. 4 I. Absolute spectral response of a typical Ag_2S target at 77 K.

II. Relative spectral response of Ag_2S after Mangalam[2].

LEGENDS TO FIGURES (continued)

Fig. 5

Fig. 5 Relative spectral transmission of a typical Ag_2S target.

Fig. 6

Fig. 6 Image of test pattern reproduced with a typical Ag_2S target at 77 K.

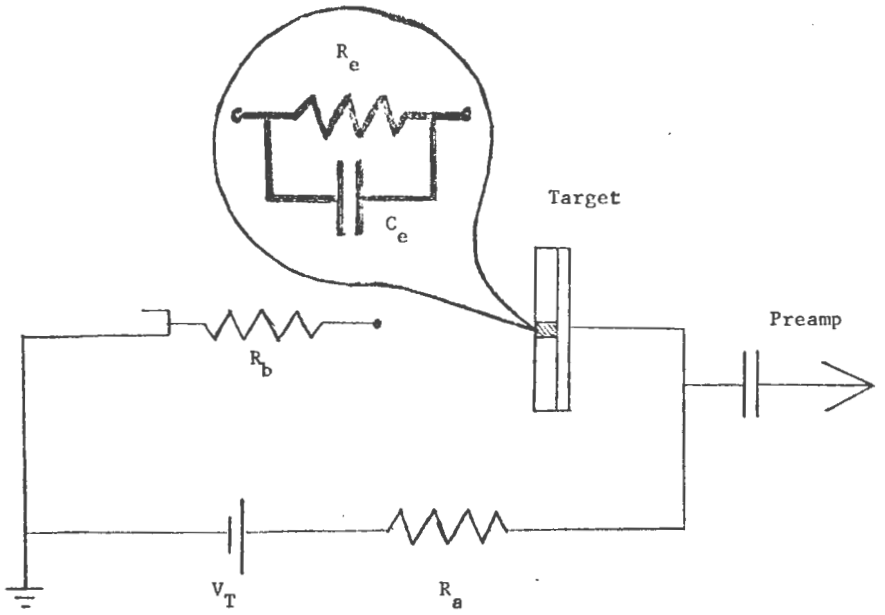

a. Schematic of a Vidicon

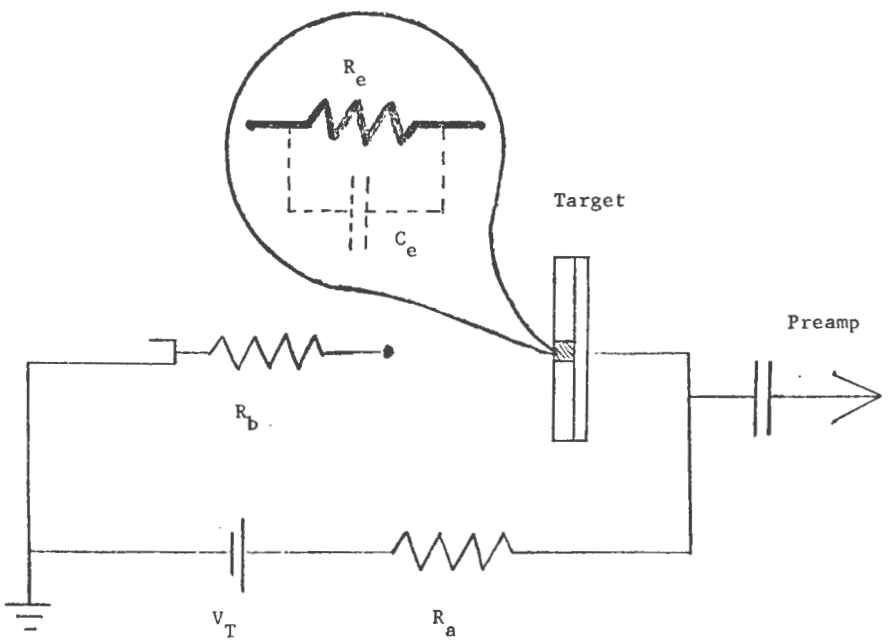

Fig. 1

b. Schematic of a Conductron

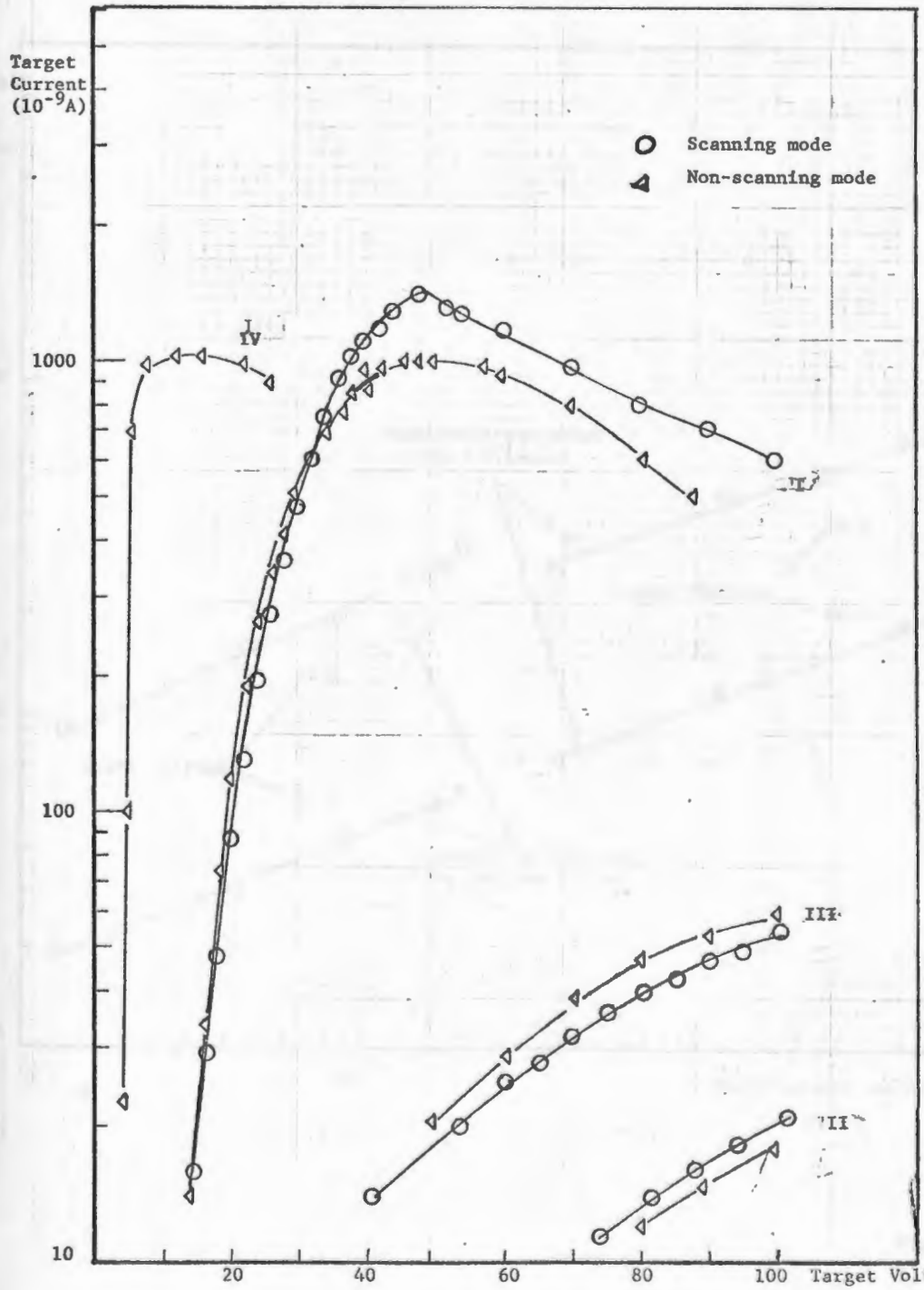
Target Current (10^{-9}A)
Scanning mode
Non-scanning mode
1000
100
10
I
IV
II
III
II
20
40
60
80
100
Target Voltage (V)

Fig. 2

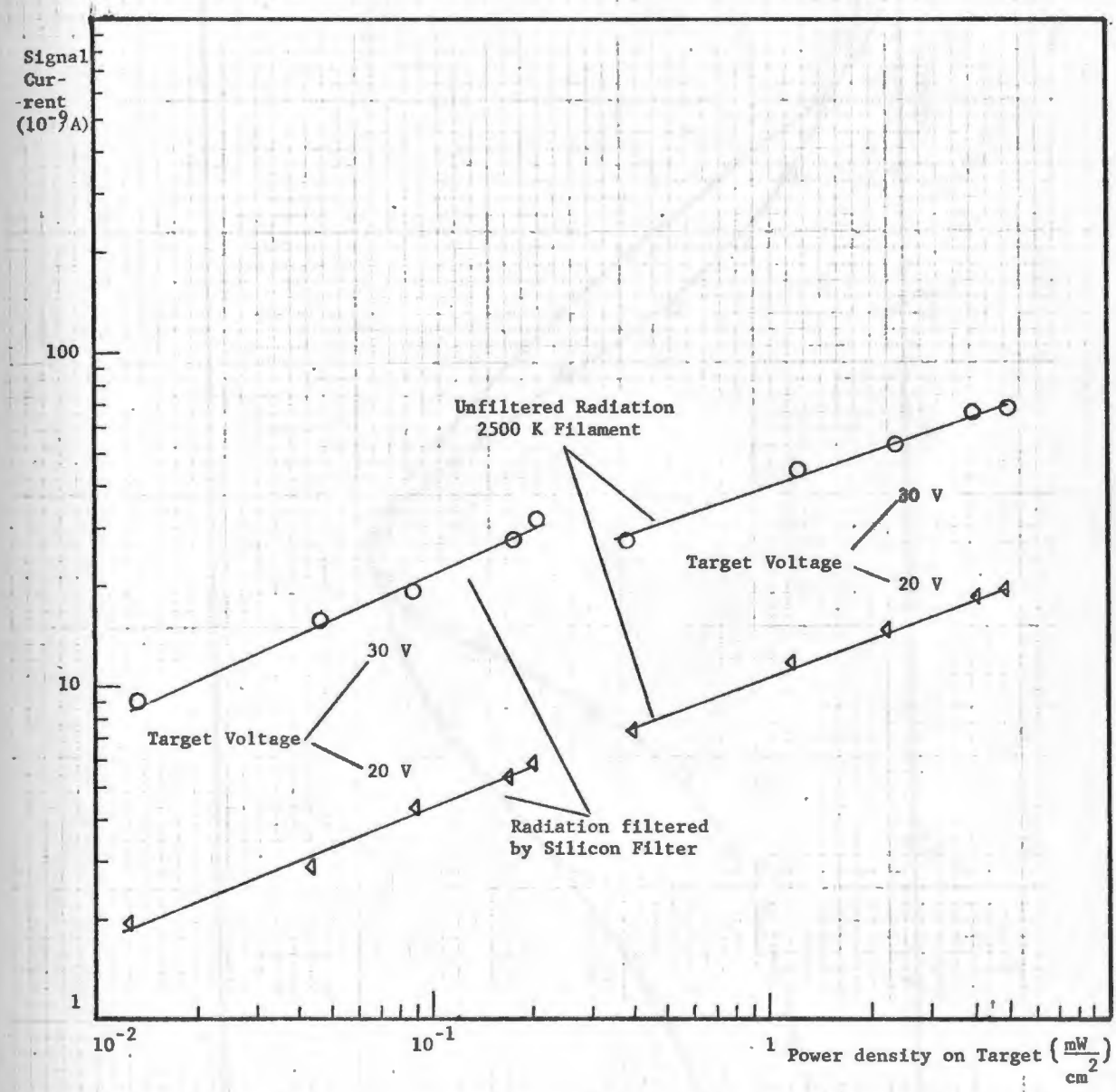
Signal Current (10^{-9}A)
100
10
1
10^{-2}
10^{-1}
1
Power density on Target ($\frac{mW}{cm^2}$)
Unfiltered Radiation
2500 K Filament
Target Voltage
30 V
20 V
Target Voltage
30 V
20 V
Radiation filtered
by Silicon Filter

Fig. 3

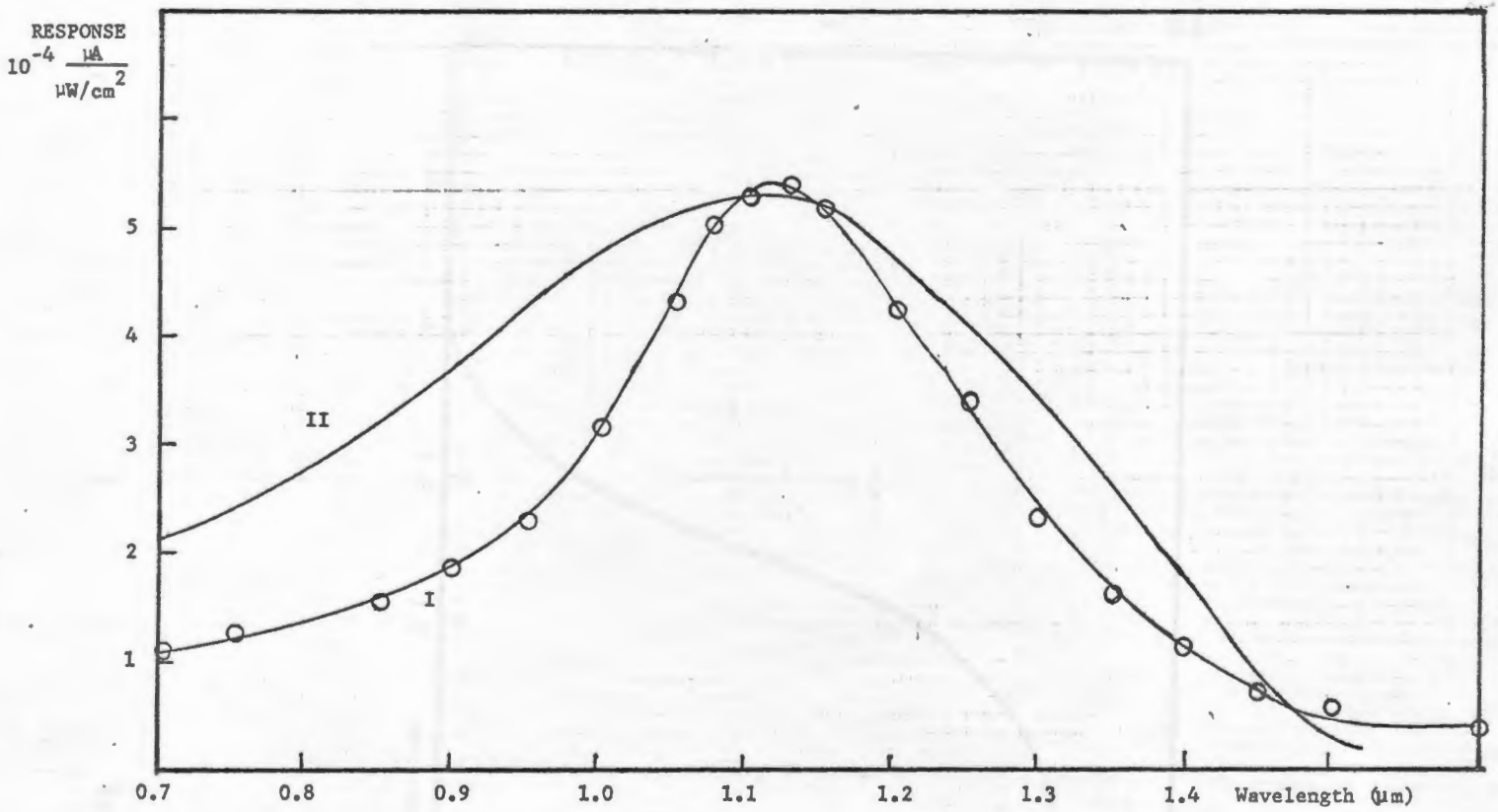
RESPONSE
10^{-4} μA / μW/cm^2
5
4
3
2
1
II
I
0.7
0.8
0.9
1.0
1.1
1.2
1.3
1.4
Wavelength (μm)

Fig. 4

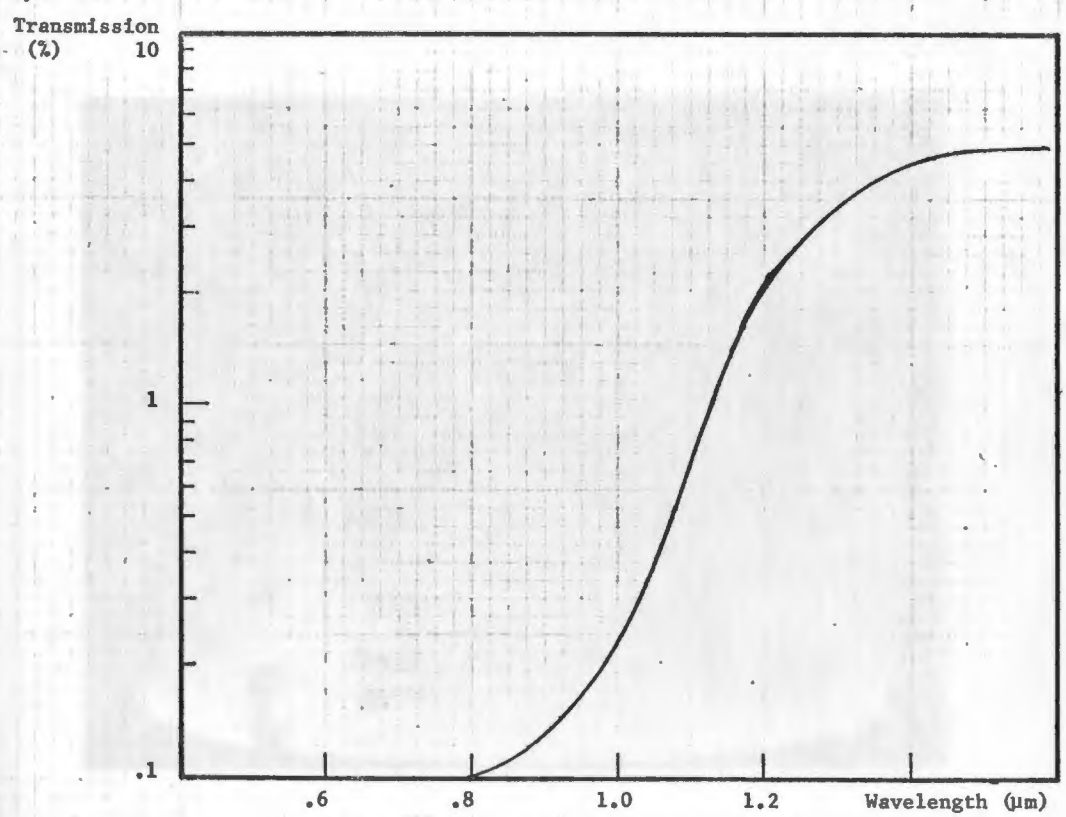

Fig. 5

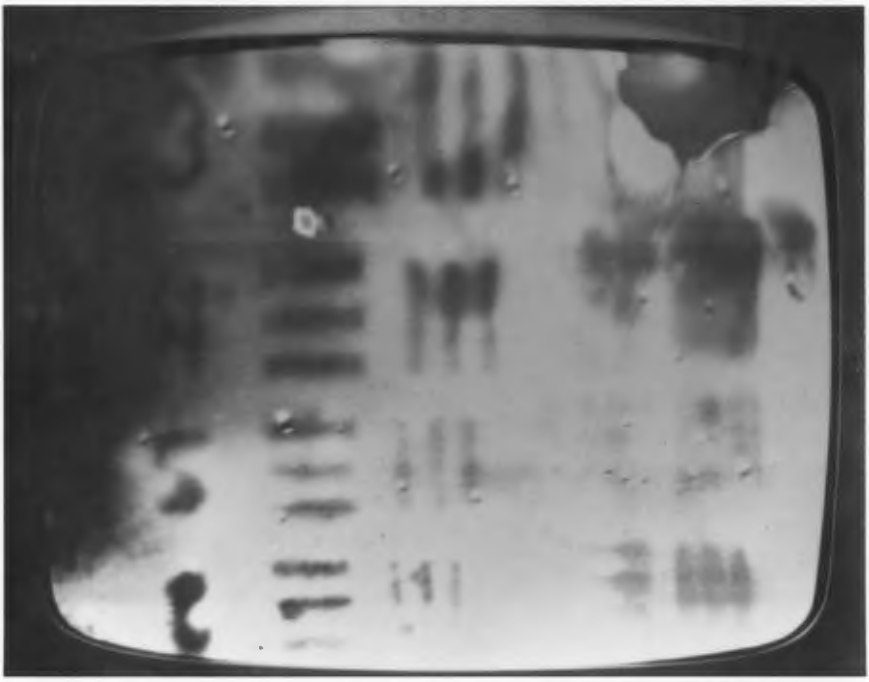

Fig. 6

BIBLIOGRAPHY

1. Coblentz, W. W., "The Effect of Crystal Structure upon Photoelectrical Sensitivity", Physical Review, Vol. 19, 1922.
2. Frueh, A. J., Jr., "The Crystallography of Silver Sulfide, Ag_2S", Zeitschrift fur Kristallographie, Bd. 110, 1958.
3. Junod, P., Helv. Phys. Acta., 32:567, 1959.
4. Mangalam, M. J., Rao, N., Suryanarayana, R., and Suryanarayana, C. V., "Electrical and Photoconductive Properties of Silver Sulphide Cells", British Journal of Applied Physics, Vol. 2, Ser. 2, 1969.
5. Mangalam, M. J., Rao, K. N., Suryanarayana, C. V., "Preparation and Characteristics of Photoconductive Silver Sulphide Layers", Indian Journal of Pure and Applied Physics, Vol. 7, 1969.
6. Djoglev, D., Andreychin, R., and Racheva, T., "Some Electric and Photoelectric Properties of Chemically Deposited Silver Sulfide Layers", Comptes rendus de l'Academie bulgare des Sciences, Tome 24, No. 2, 1971.
7. Sze, S. M., Physics of Semiconductor Devices, Wiley and Sons, 1969.
8. Rose, Albert, Concepts in Photoconductivity and Allied Problems, Interscience Publishers, 1963.

9. Bube, Richard H., Photoconductivity of Solids, John Wiley and Sons, Inc., 1960.

10. Andreychin, R. and Ivanova, H., "Positive and Negative Photovoltaic Effect in Silver Sulfide Layers", Comptes rendus de l'Academie bulgare des Sciences, Tome 15, No. 3, 1962.